universe

MDPI

Article

Optical Singly-Ionized Iron Emission in Radio-Quiet and Relativistically Jetted Active Galactic Nuclei

Paola Marziani [1,*], Marco Berton [2,3,4,†], Swayamtrupta Panda [5,6,7,‡] and Edi Bon [8]

[1] National Institute for Astrophysics (INAF), Astronomical Observatory of Padova, IT-35122 Padova, Italy
[2] European Southern Observatory (ESO), Alonso de Córdova 3107, Casilla 19, Santiago 19001, Chile; Marco.Berton@eso.org
[3] Finnish Centre for Astronomy with ESO (FINCA), University of Turku, Vesilinnantie 5, FI-20014 Turku, Finland
[4] Aalto University Metsähovi Radio Observatory, Metsähovintie 114, FI-02540 Kylmälä, Finland
[5] Center for Theoretical Physics, Polish Academy of Sciences, Al. Lotników 32/46, 02-668 Warsaw, Poland; panda@cft.edu.pl
[6] Nicolaus Copernicus Astronomical Center, Polish Academy of Sciences, ul. Bartycka 18, 00-716 Warsaw, Poland
[7] Laboratório Nacional de Astrofísica, R. dos Estados Unidos, 154-Nações, Itajubá 37504-364, MG, Brazil
[8] Belgrade Astronomical Observatory, Volgina 7, 11060 Belgrade, Serbia; ebon@aob.rs
* Correspondence: paola.marziani@inaf.it; Tel.: +39-0498293415
† ESO fellow.
‡ CNPq fellow.

Abstract: The issue of the difference between optical and UV properties of radio-quiet and radio-loud (relativistically "jetted") active galactic nuclei (AGN) is a long standing one, related to the fundamental question of why a minority of powerful AGN possess strong radio emission due to relativistic ejections. This paper examines a particular aspect: the singly-ionized iron emission in the spectral range 4400–5600 Å, where the prominent HI Hβ and [OIII]$\lambda\lambda$4959,5007 lines are also observed. We present a detailed comparison of the relative intensity of FeII multiplets in the spectral types of the quasar main sequence where most jetted sources are found, and afterwards discuss radio-loud narrow-line Seyfert 1 (NLSy1) nuclei with γ-ray detection and with prominent FeII emission. An FeII template based on I Zw 1 provides an accurate representation of the optical FeII emission for RQ and, with some caveats, also for RL sources. CLOUDY photoionization simulations indicate that the observed spectral energy distribution can account for the modest FeII emission observed in composite radio-loud spectra. However, spectral energy differences alone cannot account for the stronger FeII emission observed in radio-quiet sources, for similar physical parameters. As for RL NLSy1s, they do not seem to behave like other RL sources, likely because of their different physical properties, that could be ultimately associated with a higher Eddington ratio.

Keywords: active galactic nuclei; optical spectroscopy; ionized gas; broad line region

Citation: Marziani, P.; Berton, M.; Panda, S.; Bon, E. Optical Singly-Ionized Iron Emission in Radio-Quiet and Relativistically Jetted Active Galactic Nuclei. *Universe* **2021**, *7*, 484. https://doi.org/10.3390/universe7120484

Academic Editor: Nico Cappelluti

Received: 19 October 2021
Accepted: 1 December 2021
Published: 8 December 2021

1. Introduction

The wide majority of active galactic nuclei (AGN) are characterised by the presence of broad and narrow optical and UV lines emitted by ionic species over a wide range of ionization potential χ.[1] Restricting the attention to broad lines, type-1 AGN[2] Spectra invariably show the same low ionization lines ($\chi \lesssim 20$ eV) that include HI Balmer lines (Hβ, Hα), MgIIλ2800, the CaII IR Triplet, and FeII features, in addition to higher ionization lines (with CIVλ1549 as a prototypical representative in the rest-frame UV domain).

The relative intensities of the emission lines and their profiles do not scatter around an average, but instead change in a systematic way along the so-called quasar main sequence (MS, [4–7]). The MS can be represented in a plane where the full-width at half maximum (FWHM) of Hβ is diagrammed against the parameter $R_{\rm FeII}$, defined as the intensity ratio

between FeIIλ4570 and the broad component of Hβ that is, $R_{\rm FeII}$ = F(FeIIλ4570)/F(H$\beta_{\rm BC}$). Sketches or scatter plots of the occupation of the quasar MS in this parameter plane have been often shown in the literature (e.g., [4,7–9]). Here, we show a simple sketch of the quasar occupation in the optical parameter plane. Figure 1 identifies several spectral bins in the plane [10], and the domain of two populations: Population A, with FWHM H$\beta \lesssim 4000$ km s^{-1}, and a Population B of broader sources. The rationale for the subdivision in two Populations has been provided in several papers [5,11,12]. Population A objects are predominantly sources with high Eddington ratio, with evidence of powerful winds originating from the accretion disk [13–18]. Conversely, Population B sources have a lower Eddington ratio, and their line asymmetries are predominantly towards the red [19,20]. The origin of the asymmetry is a topic of current debate: partial obscuration and infall [21], and gravitational redshift [22–26], are two processes that have been proposed.

The importance of the $R_{\rm FeII}$ parameter stems from the fact that the FeII emission extends from UV to the IR and can dominate the thermal balance of the low-ionization broad-line region (BLR) [27]. FeII emission is self-similar in type-1 AGN but the relative intensity to Hβ (parameterised by $R_{\rm FeII}$) can vary from undetectable to $R_{\rm FeII} \gtrsim 2$, with values larger than $\approx$2 being rare (less than 1% in optically selected samples, [28]). The $R_{\rm FeII}$ trend of the MS in turn provides systematic constraints on the physical conditions of the line emitting gas [29–31], and is related to several multi-frequency properties as well. For instance, FeII emission is also correlated with narrow-line properties such as weak FeII implying strong [OIII]$\lambda\lambda$4959,5007. Boroson and Green [4] formulated this and the FWHM Hβ-$R_{\rm FeII}$ correlation in the context of the Eigenvector 1 in a principal component analysis, the main forerunner of the quasar MS, although this result was known since much earlier time (see for instance Ref. [32]). Furthermore, strong FeII is associated with a high value of the soft-X ray photon index [33–36], a tenet of the 4D Eigenvector 1 introduced by Sulentic et al. [35]. Nonetheless, a full understanding of the FeII emission remains a daunting task [30,37–39]. Even the main ionization mechanism is not fully clear. Early suggestions of a contribution of collisional ionization (e.g., [40], and references therein) have fallen into disfavour, following the extensive monitoring of several objects [41,42]: the Fe II$_{\rm opt}$ emission responds to observed continuum variations with a delay larger than the one of Hβ, but still fairly well defined.

The MS has been instrumental to the establishment of a second major result, in addition to the realisation of the importance of FeII emission. RL sources are not uniformly distributed along the main sequence [43,44]. In low-z samples, they occupy the region of low $R_{\rm FeII}$ and predominantly broad or very broad Hβ. The numbers in square brackets in Figure 1 report the fraction of sources along the sequence, and the fraction of core-dominated (CD) and Fanaroff–Riley II (FR-II) sources in each spectral bin[3]. This excludes a population of radio-detected sources that are likely associated with star formation, and are confined at the high-$R_{\rm FeII}$ end of the main sequence [45–47]. CD and FR-II sources show systematic differences, in the sense that CD sources show stronger FeII emission and narrower Balmer line [44,48,49].

In this small contribution, we focus the attention on the FeII optical spectrum of type 1 AGN, and we first provide a summary description of the optical FeII emission in the spectral region of Hβ sample (Section 2). The aim is not to solve the still-open problem of the FeII emission in type-1 AGN [30,31], but rather to establish whether the optical FeII emission might be different in radio-quiet (RQ) and RL AGN. We then present an overview of the sample used for the analysis of the differences between RQ and RL sources, keeping the distinction between CD and FR-II among jetted sources. The comparison is carried out within the MS context, namely comparing sources that are RQ and RL belonging to the same spectral type (Section 3), considering a "solid" FeII template (i.e, a template with fixed relative line intensities), and a template in which the relative multiplet strengths are free to vary (Section 4). The results (Section 5) confirm a substantial equality for the FeII emission, within the non-trivial constraints imposed by signal-to-noise ratio (S/N) and

resolution. Possible implications for the line emitting region structure in RQ and RL are briefly discussed, also with the help of photoionization computations (Section 6).

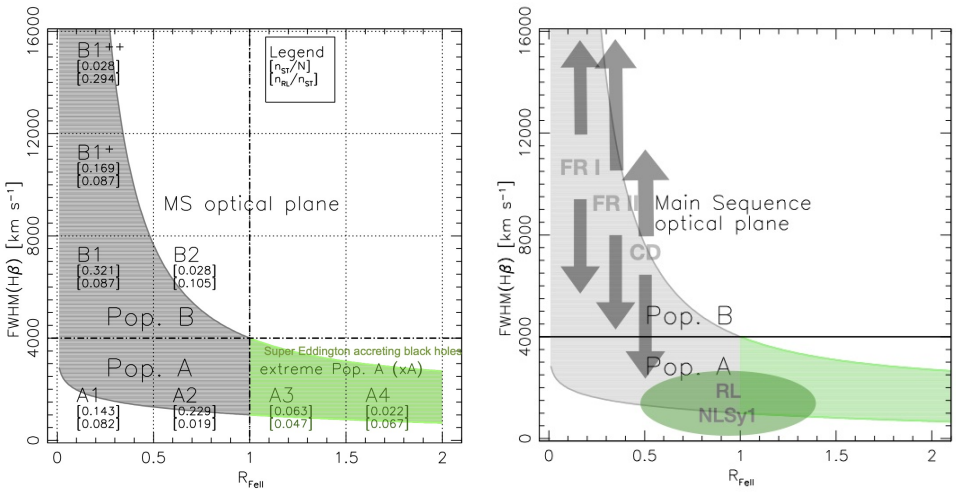

Figure 1. Left: Sketch of the optical plane of the MS, FWHM Hβ vs. $R_{\rm FeII}$. Numbers in square brackets provide, from top to bottom, the full sample fractional occupation, the fraction of RL (CD + FR-II) sources in each spectral bin. **Right**: Same section of the optical plane, but with a rough indication of the FWHM domain spanned by FR-I, FR-II, and CD along with the location of the RL NLSy1 galaxies considered in this study (dark green area).

2. The FeII Emission Lines

The main FeII optical lines in the spectral region between 4400 Å and 5600 Å are associated with five main multiplets. It is expedient to distinguish three main features:

- the blend on the blue side of Hβ, made up of lines from the m37 and m38, and usually referred to as FeIIλ4570, whose intensity is the FeII measure that enters in the definition of $R_{\rm FeII}$ and applied in most papers following Boroson and Green [4];
- m42, with two lines appearing as satellite lines of [OIII]$\lambda\lambda$4959,5007. The line at λ5018 might be affected by contamination from He Iλ5016, and is strongly affected also by the red wing of [OIII]λ5007. Given these difficulties the m42 lines were included in the fits but no result concerning this multiplet is considered;
- the lines of multiplets m48 and m49 that provide the bulk of the emission of the FeII blend on the red side of Hβ (referred to as FeIIλ5270 or as the FeII red blend).

The transitions giving rise to these lines are schematically shown in the highly-simplified Grotrian diagram of Figure 2 [3,50,51].

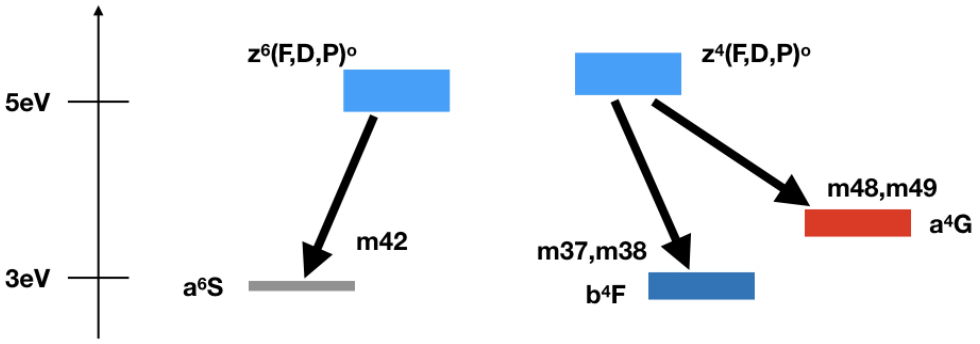

Figure 2. Highly simplified Grotrian diagram of the energy levels leading to the strongest FeII transitions in the spectral range 4400 Å–5600 Å.

The observed Fe II$_{opt}$ emission is produced by a combination of collisional and resonance-fluorescence processes [51–55]. Collisional excitation, resonance fluorescence, in which a line or continuum photon is absorbed in a line transition, both play an important role. Lyα fluorescence can populate the upper levels of Figure 2 via a population of a much higher energy level at ≈10 eV, producing a cascade with two branches leading to the z ^6D,^6F,^6P,^4D, ^4F, and ^4P terms between 4.8 and 5.6 eV responsible for the optical emission between 4500 and 5600 Å. Collisional excitation, albeit significant [56], alone cannot explain the emission of the stronger FeII emitters.

3. Sample

This paper considers two samples of broad-line, type-1 sources:

- a sample of bright quasars from the Sloan Digital Sky Survey (SDSS) database in the redshift range $0.4 \lesssim z \lesssim 0.7$ [28,57]. Composite median spectra were extracted for the RQ, CD and FR-II radio classes. A significant number of RL sources (out of the 680 quasars of the original sample) are found only in the spectral bins A1, B1, B1$^+$: 8, 16, 9 CDs and 10, 23, 11 FR-IIs in each bin, respectively. All sources (save a borderline one) in the sample that are RL with extended emission satisfy the power criterion at 1.5 GHz $\log P\nu \gtrsim 31.7$ erg s^{-1} Hz^{-1} that separate FR-II sources from the lower luminosity FR-I [58,59].[4] In the last bin, however, the FeII intensity is consistent with 0, so that only sources in bin A1 and B1 are considered. In addition, in A1 FR-II the Fe II$_{opt}$ emission is too weak for a meaningful analysis. In conclusion, our bright quasar sample belongs in the following composite spectra: A1 RQ, A1 CD, B1 RQ, B1 CD, B1 FR-II;
- three individual relativistically jetted NLSy1s with γ-ray detections, that show more prominent FeII emission than the composites. The γ-ray detection supports the presence of a relativistic jet as the origin of the radio power for these sources [61]. They were selected because high-quality optical spectra were available for the three of them.

The three γ-ray sources are 1H 0323+342 (≡B2 0321+33 ≡ 1H 0323+342 ≡ J03246+341), 3C 286 (≡J13311+305), and PKS 2004-447 (≡J20079–445). J03246 is the closest γ-ray NLSy1 ($z = 0.063$), hosted either by a spiral or an interacting late-type galaxy [62,63], and it is the only known γ-NLSy1 showing a Fe Kα emission line in X-rays [64]. This object was detected by the *Fermi* Gamma-ray Space Telescope soon after its launch [65]. J13311 is a rather high redshift ($z \approx 0.850$) object, identified as a γ-ray source in all *Fermi* catalogs (e.g., [66]). Originally it was classified as a compact steep-spectrum (CSS) source based on its radio morphology [67], and later as a NLSy1 from optical spectroscopy [68,69]. Also J20079 ($z \approx 0.240$) is classified as both a CSS and a NLSy1 [70–72] and, as J03246, it belongs to the first batch of NLSy1s detected by *Fermi* [65]. The spectra of these three sources were obtained using the Asiago 1.22m Telescope for J03246 (full description of the data reduction in Foschini et al. [73]), the SDSS archive for J13311, and the FORS2 instrument on the Very Large Telescope for J20079–445 [72].

4. Analysis

The analysis is mainly empirical and, as mentioned, there is no pretension to solve the problem of the optical FeII emission in AGN. Two approaches are followed in the measurement of the relative intensity of the multiplets:

- the modelling of the spectrum using a "solid" FeII template, scaled and broadened to minimise the χ^2 in a multi-component fit. It is basically the one of Boroson and Green [4] actualised with a higher resolution spectrum and a model of the FeII emission underlying Hβ [20]. In this case, a multi-component fit was carried out including all known emission components, as detailed in several recent works [74–76]. Specifically, the redward asymmetric Hβ has been modelled by the use of three components—a narrow, a broad and a very broad component ([77], and references therein). After

verification that the host galaxy spectral emission is not contributing significantly, the local continuum was fit with a power law;

- the use of a "liquid" template that permits to change the relative intensity of the multiplets in the optical spectral range [78,79] [5] In this case, the continuum subtracted spectrum was fit to a set of variable multiplets and to Hβ and [OIII]λ5007 profiles that were approximated as Gaussians.

5. Results

5.1. FeII Emission Comparison between RQ and RL

The results of the application of the multi-component fit with the solid FeII template are shown in Figures 3 and 4 for the spectral types A1 and B1, respectively. In Figure 3, the only comparison we show is between A1 RQ and A1 CD sources, as there is no A1 FR-II composite. In Figure 4, the left panel shows the comparison between B1 RQ and B1 CD composites, while on the right the B1 RQ composites are compared to B1 FR-II. The immediate result is that RL (CD and FR-II) composites show weaker FeII emission [44]. The second immediate result [already reported in 19] is the similar appearance of the Hβ profiles. The Hβ profiles of Figures 3 and 4 confirm that the prominent redward asymmetry is not a prerogative of RL sources, but is a common feature in *both* RQ and RL sources, provided that they belong to Population B [11,80,81].

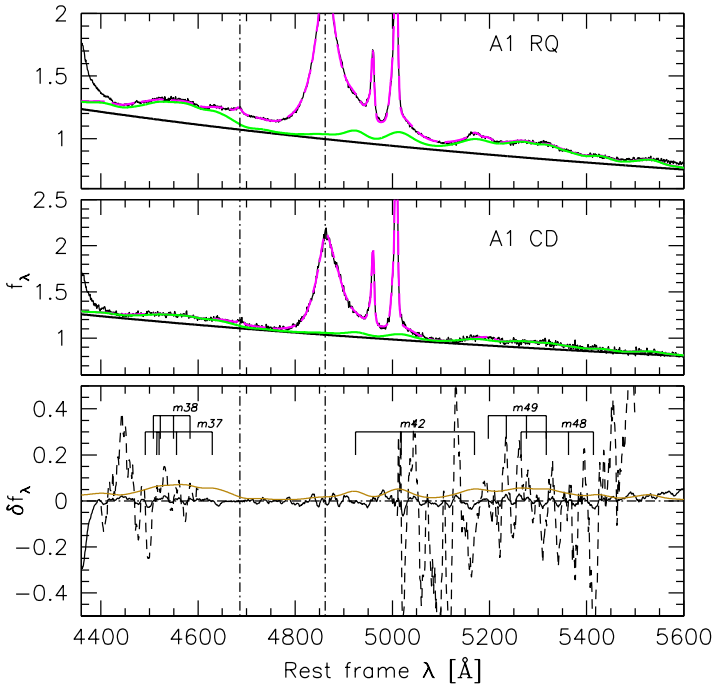

Figure 3. From top to bottom: Non-linear χ^2 multi-component analysis with a solid FeII template of RQ, CD, and of the residuals in FeII emission for composites of spectral type A1. In the bottom panel the brown line traces the difference in the template (positive, since FeII is stronger in RQ than in CD). The black filled lines traces the difference between the observed FeII emission after rescaling of the CD FeII to obtain a minimum average ∼0. The dashed line traces the relative difference, i.e., (FeII RQ − FeII CD)/FeII RQ. Wavelengths of multiplet lines are from Moore [82].

The bottom panels of Figures 3 and 4 provide constraints on the nature of the difference between FeII emissions in the RQ and RL composite spectra. The brown line traces the difference in the templates, which is positive since FeII is stronger in RQ than in CD and FR-II as well. The black filled lines traces the difference between the observed FeII emission after rescaling of the RL FeII emission by a factor k to obtain an average of 0. The difference is computed between the observed FeII spectra, as follows:

$$\delta \mathrm{FeII}_{\lambda,\mathrm{i}} = f_{\lambda,\mathrm{rq}} - (\mathcal{M}_{\lambda,\mathrm{rq}} - Fe_{\lambda,\mathrm{rq}}) - k_{\mathrm{i}} \cdot [f_{\lambda,\mathrm{i}} - (\mathcal{M}_{\lambda,\mathrm{i}} - Fe_{\lambda,\mathrm{i}})] \quad (1)$$

$$\frac{\delta \mathrm{FeII}_{\lambda,\mathrm{i}}}{Fe_{\lambda,\mathrm{rq}}} = \frac{f_{\lambda,\mathrm{rq}} - (\mathcal{M}_{\lambda,\mathrm{rq}} - Fe_{\lambda,\mathrm{rq}}) - k_{\mathrm{i}} \cdot [f_{\lambda,\mathrm{i}} - (\mathcal{M}_{\lambda,\mathrm{i}} - Fe_{\lambda,\mathrm{i}})]}{Fe_{\lambda,\mathrm{rq}}}, \quad (2)$$

where the index i refers to CD or FR-II, the f_λ to the observed flux as a function of wavelength, and the calligraphic symbols refer to model spectrum ($\mathcal{M}_\lambda$) and model FeII (Fe) via the scaled and broadened template. Model parameters were obtained with a multi-component, non-linear minimum χ^2 technique, as implemented in IRAF [83].

The basic results of the spectral fits are reported in Table 1. The Table columns list, in the following order, the spectrum identification, the rest-frame equivalent width in Å for FeIIλ4570, R_{FeII}, FWHM Hβ, the spectral type defined on the basis of the reported R_{FeII} and FWHM Hβ, and the rescaling factor k.

Table 2 lists the average of the absolute difference between the observed iron blends and the solid FeII template. The averages are computed over the full ranges 4434 Å–4684 Å (hereafter indicated as B blend or FeIIλ4570), and 5100 Å–5600 Å (hereafter R blend) also used for the CLOUDY photoionization simulations (Section 6.1). The next columns yield the average and relative absolute differences between RL and RQ after rescaling, for the restricted spectral region $\tilde{B}$ between 4500 and 4590 Å (roughly corresponding to multiplets 37 and 38) and $\tilde{R}$ (between 5200 and 5330 Å, with the strongest features of m48 and m49). The reason of this restriction is to avoid the contamination by HeII on the blue side of Hβ. The HeIIλ4686 line can have a significant effect and its estimation is based only from fit.

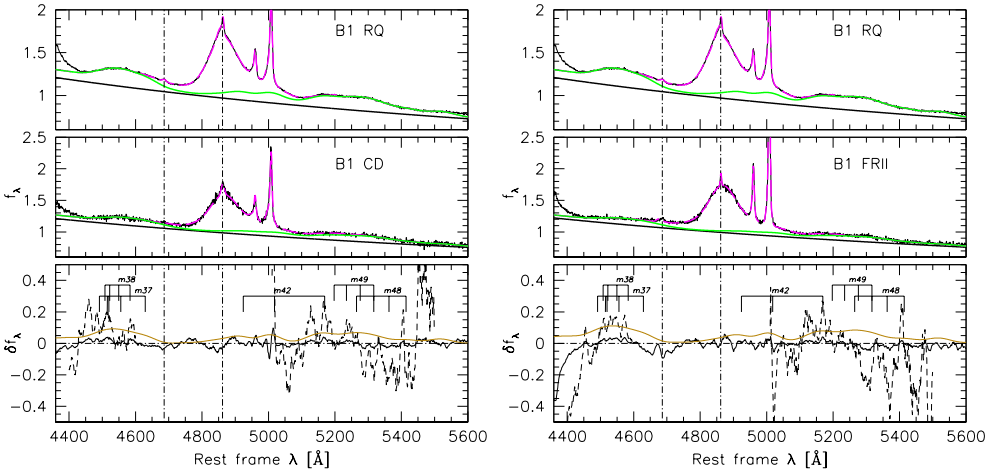

Figure 4. In the left panel, comparison between RQ and CD composites of spectral type B1. In the right panel, comparison between B1 RQ, the same as in the left panel, and B1 FR-II. Bottom panels as in Figure 3.

Table 1. Basic results.

Spectrum	W(FeIIλ4570)	R_{FeII}	FWHM Hβ	ST	k
Composite spectra					
A1 RQ	31.6	0.291	3230	A1	…
A1 CD	16.2	0.397	3290	A1	1.815
B1 RQ	44.1	0.414	6940	B1	…
B1 CD	26.0	0.281	7060	B1	1.657
B1 FR-II	21.5	0.184	6790	B1	1.900
FeII template	…	…	990	A	…
γ RL NLSy1s					
1H 0323+342	50.1	1.03	1280	A3	…
3C 286	33.5	0.792	3170	A2	…
PKS 2004-447	36.7	0.5455	1470	A2	…

Table 2. FeII results.

Spectrum	$\overline{f_\lambda - \mathcal{M}_\lambda(B)}$ [a]	$\overline{f_\lambda - \mathcal{M}_\lambda(R)}$ [b]	$\overline{\delta f_\lambda(\tilde{B})}$ [c]	$\overline{\delta f_\lambda / f_\lambda(\tilde{B})}$ [c]	$\overline{\delta f_\lambda(\tilde{R})}$ [c]	$\overline{\delta f_\lambda / f_\lambda(\tilde{R})}$ [c]
Composite spectra						
A1 RQ	0.00146 ± 0.00942	0.00257 ± 0.01333	...	...	...	...
A1 CD	0.00014 ± 0.01265	-0.00117 ± 0.01671	0.00244	-9.986×10^{-5}	0.0146	−0.00354
B1 RQ	0.00149 ± 0.00665	0.00277 ± 0.00982	...	...	...	...
B1 CD	-0.00188 ± 0.01698	$9.44 \times 10^{-5} \pm 0.01745$	0.01420	0.07467	−0.00403	−0.02626
B1 FR−II	0.00297 ± 0.01554	0.0047 ± 0.01574	0.03138	0.15740	−0.00294	−0.01834
γ RL NLSy1s						
1H 0323+342	0.00509 ± 0.05126	0.00949 ± 0.04280	−0.00598	−0.0388	0.02072	0.1297
3C 286	-0.00262 ± 0.03654	0.005087 ± 0.05126	−0.00304	−0.0254	0.00516	0.0475
PKS 2004−447	-0.00145 ± 0.02275	0.005514 ± 0.02115	−0.0008	−0.0149	0.00866	0.1117

[a]: Averages of the normalised flux difference between the continuum subtracted spectrum and the solid template in the range 4434–4684 Å; [b]: same, in the range 5100–5600 Å; [c]: absolute and relative average difference following Equations (1) and (2), for the restricted B and R ranges, respectively.

In the case of spectral type A1, the comparison between RQ and CD relative intensities of the multiplets is shown in the panels of Figure 3. On the blue side, the $\delta\mathrm{FeII}_{\lambda,\mathrm{i}}$ is consistent with 0 over the range where most of the emission due to multiplets 37 and 38 is expected. Similar considerations apply to the red side emission; the main fluctuations according to Equation (2) occur when FeII emission is weak.

The comparison for the composite spectra of bin B1 is shown in Figure 4. On the blue side of Hβ in correspondence of the m37 and m38 emission there could be a slight excess for the CD composite, accompanied by a deficit on the red side of Hβ where emission is associated with multiplets m48 and m49. The average relative difference is a few positive and negative percents for the B and R regions, respectively (Table 2). Accepted as real the absolute difference is constrained within $\lesssim$3%, and the relative difference is contained within ±20%. The ≈3% average excess translates into an error in terms of $\delta R_{\mathrm{FeII}} \approx 0.03$, and in W FeIIλ4570 the difference is also ≈3 Å implying that there is no effect on the placement in the MS optical plane. To estimate the measurement errors on R_{FeII} for the same S/N, equivalent width and FWHM of the lines, we used the quality parameter defined in an unrelated investigation, and derived from Monte Carlo simulations estimates of the errors for Hβ and R_{FeII}. The errors on FeII are the dominant one, and are $\delta R_{\mathrm{FeII}} \lesssim 0.05$ for the RQ composites and $\delta R_{\mathrm{FeII}} \approx 0.10$ for the radio-loud ones.

5.2. γ-ray Detected RL NLSy1s

We apply the same fitting techniques to three relativistically jetted NLSy1s with γ-ray detection. Figure 5 shows that the solid template used for the fitting of the composites is providing a good agreement, in a case with higher values of R_{FeII} and much narrower lines that is better posed to appreciate possible differences. The fits are successful, and the residuals consistent with 0, with average systematic differences are $\lesssim$1%, and the rms scatter is $\lesssim$5% of the normalised continuum value at 5100 Å.

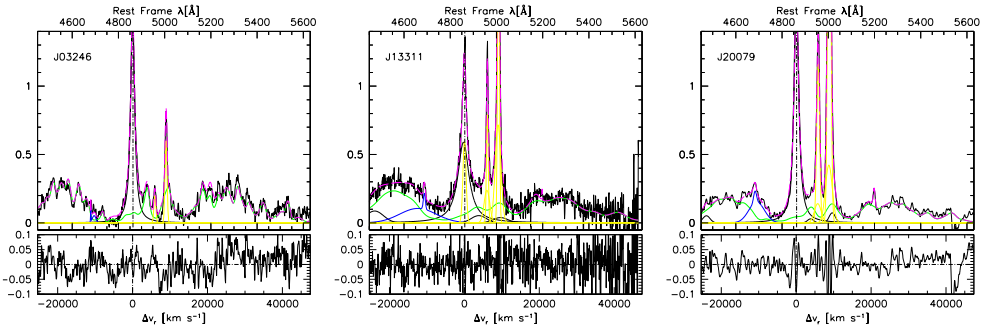

Figure 5. Non-linear χ^2 multi-component analysis with a solid FeII template (green) of three jetted NLSy1s with γ-ray detections. The spectra are shown after continuum subtraction. The thin filled line traces the observed spectrum. The dashed magenta line represents the model, and the thick black line the H$\beta_{\rm BC}$. The [OIII]$\lambda\lambda$4959,5007 is shown in yellow. The lower panel show the residuals of the subtraction of the model from the observed spectrum. From left to right panel, J03246+341, J13311+305, and J20079-445.

5.3. Models with Relative Intensity of the Multiplets Free to Vary

We first considered the measurements based on the continuum-subtracted spectra in the full and restricted ranges (second and third columns of Table 3), and we utilised the web-based fitting tool[6] for implementing the scheme of Kovačević et al. [78] for the optical FeII emission. The measurement of the ratio between the sum of the m37+m38, and m48+m49 blends is reported in the fourth column of Table 3. The fifth column reports the ratio $\tilde{B}_{\rm k}/\tilde{R}_{\rm k}$ measured on the full spectral model of Kovačević et al. [78]. The last two columns report the average differences between the observed and the Kovačević et al. [78] modelling for the restricted ranges $\tilde{B}_{\rm k}$ and $\tilde{R}_{\rm k}$, respectively, and are meant to provide an estimate of how well the model FeII reproduces the actual observations. The agreement is very good with all cases having the average difference less than 0.05, and most less than 0.01. The same procedure was also applied to the solid FeII template used in the previous analysis (Figure 6). The values reported in Table 3 explain why the solid FeII template provides satisfactory results in all cases, and especially in the RQ cases.

Table 3. "Liquid" FeII results.

Spectrum	B/R [a]	$\tilde{B}/\tilde{R}$ [b]	$\frac{m37+m38z}{m48+m49}$ [c]	$\tilde{B}_{\rm k}/\tilde{R}_{\rm k}$ [d]	$\overline{\tilde{B}-\tilde{B}_{\rm k}}$ [e]	$\overline{\tilde{R}-\tilde{R}_{\rm k}}$ [e]
Composite spectra						
A1 RQ	0.993	0.994	0.82	0.974	0.00447	−0.0182
A1 CD	1.141	1.045	0.72	0.942	0.0117	0.0075
B1 RQ	0.884	0.891	0.97	0.899	0.00934	0.00419
B1 CD	0.666	0.698	0.79	0.699	−0.0375	−0.0198
B1 FR−II	0.685	0.726	0.65	0.890	−0.051	−0.0169
FeII template	0.792	0.979	0.65	0.967	0.00264	0.00813
γ RL NLSy1s						
1H 0323+342	0.743	0.780	0.59	0.765	0.0048	−0.00020
3C 286	0.821	0.905	0.78	0.867	0.00591	−0.00218
PKS 2004-447	0.980	0.882	0.62	0.882	0.00093	−0.0000466

[a]: B/R ratio measured on the observed spectrum; [b]: same as in the previous column, but $\tilde{B}/\tilde{R}$ in the restricted range; [c]: ratio between the sum of m37+m38 and m48+m49 intensity obtained with the fits following Kovačević et al. [78]. Note that the ratio includes only the sums of these four multiplets, while both the standard and the restricted range include additional FeII emission as well as a possible residual contribution of HeI and HeII lines. [d]: ratio between the FeII emission of the B and R restricted range computed with the simulations of Kovačević et al. [78]. [e]: absolute average difference for the restricted B and R ranges, respectively, using the *total* FeII emission following Kovačević et al. [78].

We stress three main results:

- There is a significant difference (by a factor ≈2) between RQ and RL sources in the same spectral types (meaning similar mass, Eddington ratio $\lesssim$0.1, and luminosity);
- The B/R ratio for the RQ A1 and B1 spectral types is ≈0.9–1.1 (Figure 7 and Table 3);

- The various measurements of the blue and red blend ratios suggest a somewhat higher values for the A1 and B1 RQ than for the RL sources (≈0.9–1 vs. 0.7). The effect is not strong: yet, it is apparent especially in Figure 7.

It is advisable to consider that there could be effects not related to the estimation of the FeII intensity. The main reason could be a difference in the intensity of HeIIλ4686, even if HeIIλ4686 is included in the fit. Other possibilities involve internal extinction [84,85] affecting the FeII emitting region, limb-darkening [6], incorrect continuum placement, contamination by lines other than HeII, and blueshifted Hβ emission. To overcome at least the problem of the HeIIλ4686 uncertain contribution, and of the contribution of the Hβ wings, we defined a restricted range for B and R, $\tilde{B}$ and $\tilde{R}$. The effect is, however, not significantly reduced (Table 2).

If we apply the same technique to the γ-detected sources, the intensity ratio between B and R is closer to the value of the template (Figure 8 and Table 3) but not for 1H 0323+342. The values reported in Table 3 confirm that the template is providing a good approximation for the RQ sources in bin A1 and B1. This is likely also true for spectral bins with higher $R_{\rm FeII}$ (A2 and A3), as the template is based on the spectrum of I Zw 1, a NLSy1 accreting at a high rate and especially emitting strong FeII, with $R_{\rm FeII}$ slightly larger than 1, and so of spectral type A3[7]. At the other end of the MS, FeII emission is faint and systematic differences might be not appreciable. So the issue of a possible, significant disagreement concerns only ≈3% of all type 1 AGN.

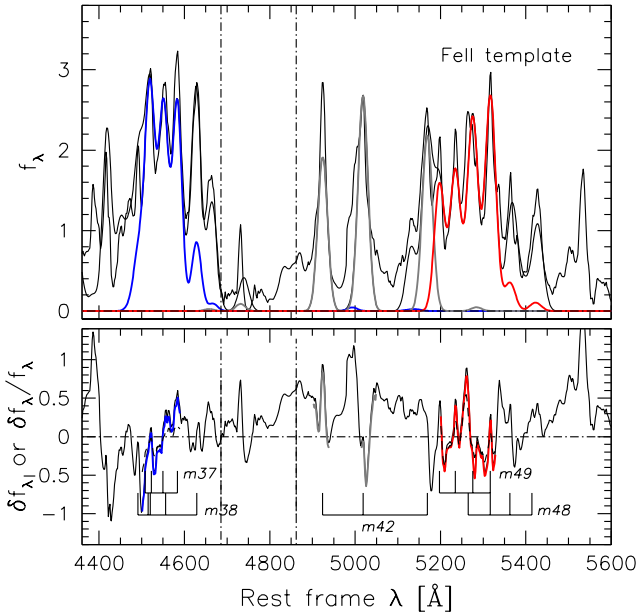

Figure 6. Non-linear χ^2 multi-component analysis of the adopted solid FeII template with relative multiplet intensity free to vary. The blue solid line represents the B blends, while the red solid line indicates the R blends.

In summary, the use of a solid FeII template appears fully justified in this work. There could be a genuine effect associated with radio-loudness, in the sense of a less prominent blue blend with respect to the red one.

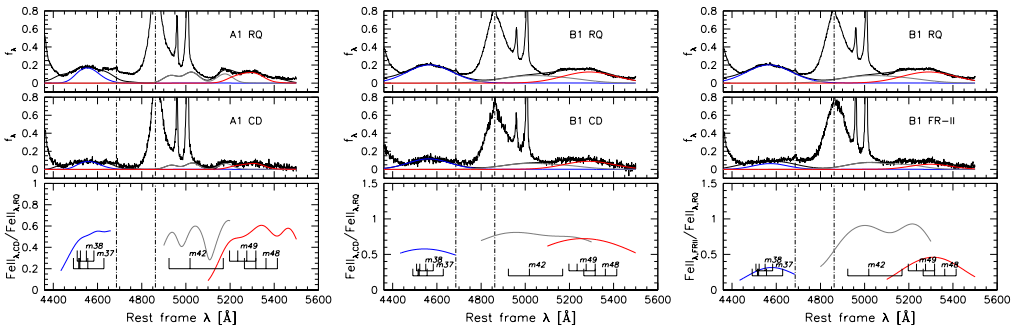

Figure 7. Non-linear χ^2 multi-component analysis with a FeII template with relative multiplet intensity free to vary. Colours as in Figure 6.

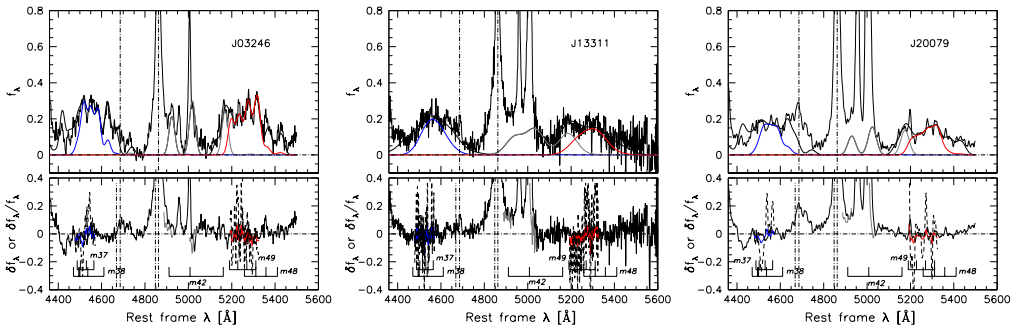

Figure 8. Non-linear χ^2 multi-component analysis with a FeII template with relative multiplet intensity free to vary, from left to right for the A1 RQ vs. A1 CD, B1 RQ vs. B1 CD, B1 RQ vs. B1 FR-II composites. The bottom panels show the ratios between the B, m42, and R for the three cases. Colours as in Figure 6.

6. Discussion

The composites that we have considered in the present work all show modest FeII emission and satisfy the condition that $R_{\rm FeII} \lesssim 0.5$. In principle, on the context of photoionization, they do not pose a serious challenge to the conventional view of the of the BLR as a system of emitting clouds characterised by typical densities $n_{\rm H} \sim 10^{9.5}$ cm^{-3}, and column density $N_{\rm c} = 10^{23}$ [cm^{-2}] [87]. Indeed, physical parameters similar to these $n_{\rm H} \sim 10^{10-10.5}$ cm^{-3}, along with metallicity solar or slightly sub-solar, and a flattish spectral energy distribution (SED) [88,89], can account for the emission in the $R_{\rm FeII}$ range of spectral bins A1 and B1, at BLR distances from the continuum sources consistent with their luminosity [31].

Thanks especially to the results of reverberation mapping and [27], the emitting region radius was found to be a factor of 10 smaller than previously thought [90,91]. The conventional view outlined in the previous paragraph may be only partially valid in Population A sources, as it is unable to account for the strong FeII emission in quasars [92,93]. Different physical conditions are required for sources with stronger FeII emission: higher densities are needed to maintain the ionization parameter within reasonable limits. In spectral type A3, $n_{\rm H} \sim 10^{12}$ cm^{-3} (strong FeII emission appears possible only if $n_{\rm H} \gtrsim 10^{10.5}$ cm^{-3}, [30,94,95]). High column density and super-solar metallicity provide a further boost to the FeII intensity and to the strength of the metal lines in the UV [30,96].

6.1. Photoionization Computations

To ascertain the role of the SED in the strength of FeII we performed exploratory calculations of the RQ and RL differences, as well as for the γ-detected NLSy1s. As a first attempt, we assumed a column density $N_{\rm c} = 10^{23}$ cm^{-2}, solar metallicity, and 0 micro-turbulence. We focused on the exploration of the parameter ranges of the density

$n_{\rm H}$ ($\sim 10^{9-11}$ cm^{-3}), and of BLR radius within the range expected from the Bentz et al. [97] scaling law, corrected for high-accretion rates ([98,99]; see also [100]). We utilised the SEDs from Laor et al. [88] and Korista et al. [89], which are most appropriate for bins A1 and B1, for RQ and RL separately (top panel of Figure 9). The two RQ SEDs most likely bracket the distribution of SEDs in the two bins, as also assumed in previous work [31]. For the composites, we consider a fixed luminosity $\lambda L_\lambda(5100\ \text{Å}) \approx 10^{45}$ erg s^{-1}, consistent with the values derived for the original sample [28]. For RL NLSy1s, we built a specific SED for each one of them by using the multi-frequency data of the SED builder available at the Space Science Data Centre of the Italian Space Agency[8] The results are shown in the second, third, and fourth panel of Figure 9.

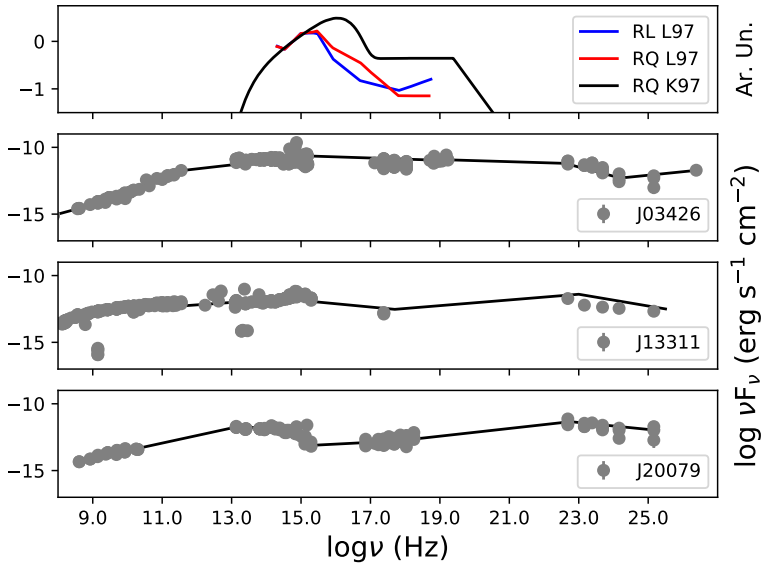

Figure 9. The SEDs used for photoionization computations. From top to bottom: (1) SED of RL and RQ sources from Laor et al. [88], represented by the blue and red solid line, respectively, and from Korista et al. [89] for RQ shown with black solid line. The y-axis for the upper panel is shown with arbitrary units (Ar. Un.) for the specific flux; (2) SED of J03426. The observed data points are shown in grey, while the SED used in the models is represented by the black solid line, (3) as in (2) for J13311; (4) as in (2) for J20079.

6.2. Composites RL and RQ

Figure 10 shows the expected $R_{\rm FeII}$, the ratio between the red blend R and Hβ, and the ratio B/R for the RQ and RL SEDs, as a function of $r_{\rm BLR}$ and $n_{\rm H}$. As mentioned above, the range in $r_{\rm BLR}$ has been centred on the value expected from the correlation $r_{\rm BLR}$-L by Bentz et al. [97]. The density range includes the most likely values for the BLR along the MS. Typical values are lower for Population B, and much higher for Population A. [6,101].

The most important result is that *the SED for RL sources is able to account for the modest* $R_{\rm FeII}$ *and* W(FeIIλ4570) reported in Table 1. The observed equivalent width $\sim$10–20 Å and $R_{\rm FeII} \sim 0.15$ are explained at the $r_{\rm BLR}$ expected from the $r_{\rm BLR}$-L relation, and by the moderate density $n_{\rm H} \sim 10^{11}$ cm^{-3}. The result seems to be especially robust against changes in $n_{\rm H}$ and $r_{\rm BLR}$ (Figure 10, middle column). Restricting the ranges to $\tilde{B}$ and $\tilde{R}$ confirms this conclusion (Figure A1; the result of the analysis for the restricted range are shown in Appendix A).

Regarding the interpretation of the composite spectra, a second important issue is whether the difference in RQ and RL SED can explain the differences in their FeII strength. We stress that the comparison is being carried out between sources that are in the same spectral types, meaning that they have similar $M_{\rm BH}$, L, and Eddington ratio. The $R_{\rm FeII}$ computed over a large area of the parameter plane $n_{\rm H} - r_{\rm BLR}$ shows differences that are at most 0.05, i.e., less than 15% (Figure 10). This has the important implication that the parameter $k \approx 2$, *that is,* $R_{\rm FeII}$ *twice as strong in RQ than in RL AGNs, cannot be explained on the*

basis of the SED only. However, the RQ SED that we adopt is not necessarily equivalent to the one of the sources used to construct the Population A and B. Using the SED from Korista et al. [89] that has a stronger *big blue bump* (implying for fixed $r_{\rm BLR}$ and $n_{\rm H}$ an increase in ionization parameter by a factor 3) cannot lead to a higher $R_{\rm FeII}$ (Figures 11 and A2).

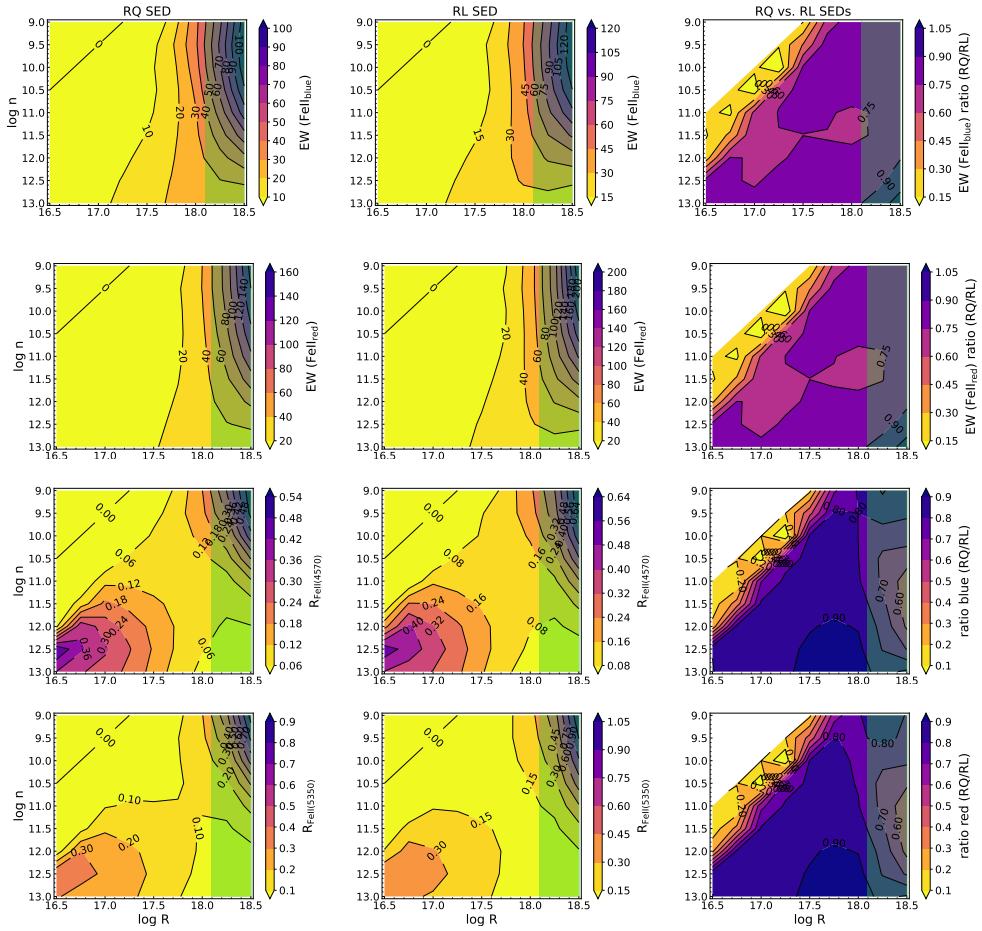

Figure 10. Results of CLOUDY simulations. First two rows: W(FeIIλ4570) for RQ and RL (i.e., computed for the same physical parameters but with the two different SEDs of Laor et al. [88]) and their ratios; third and fourth row from top: $R_{\rm FeII}$, for RQ and RL and their ratios. Last four rows: same, for the red (R) FeII blend peaked at λ 5312 Å.

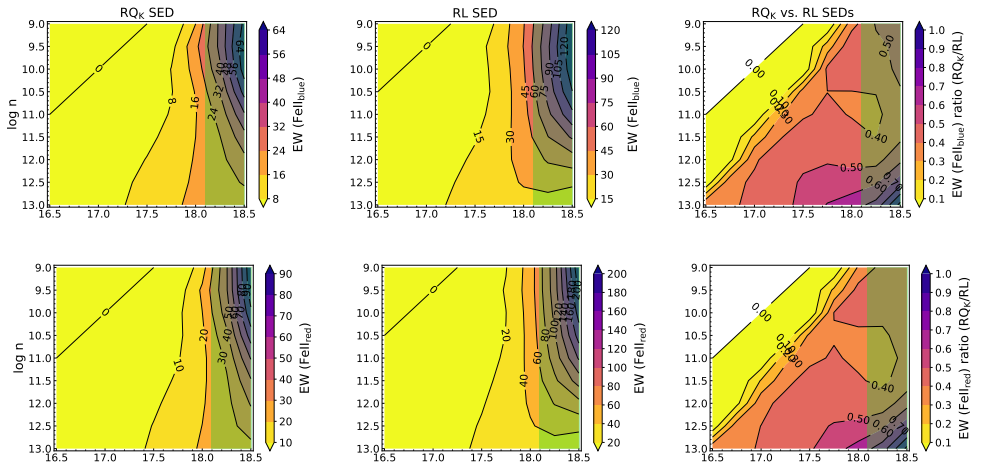

Figure 11. *Cont.*

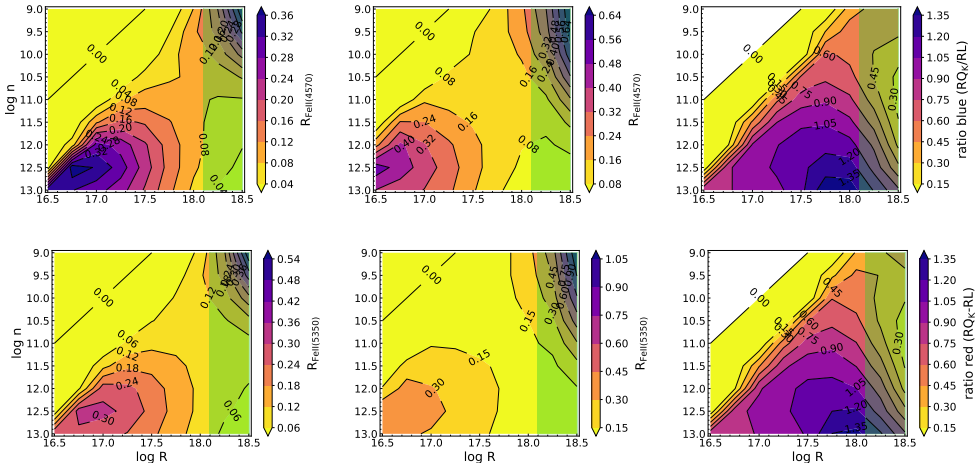

Figure 11. Results of CLOUDY simulations, the same as in Figure 10 but for the RQ SED of Korista et al. [89].

The second issue investigated in the present paper is the possibility of a systematic difference in the B/R FeII ratio. This result should be viewed with care, and confirmatory data are needed, also considering that we are dealing mainly with weak FeII emitters. The agreement between the observed and photoionization-predicted B/R is good, and in most cases the B/R $\sim$ 1, with little dependence on the $r_{\rm BLR}$ and $n_{\rm H}$ parameters. Figure 12 (Figure A3 for the restricted ranges) shows that there is a possible lowering of the B/R ratio in the B1 RL (both CD and FR-II) with respect to the RQ. Accepted at face value, it might imply a lower density, and a higher ionization parameter for the RL sources (Figure 12), although Figures 10 and 11 show that this implies fainter FeII emission than what is expected for the typical values of $r_{\rm BLR}$.

Sulentic et al. [102] speculated that the cocoon associated with the shock wave due to the expansion of the jet could push outward the line emitting regions. It is known that the CIV high-ionization line reaches lower blueshift amplitudes in RL than in RQ sources [14,103]. The present paper confirms that an effect on the low-ionization lines is minor. Considering the layout of the atomic levels in the Grotrian diagram of Figure 2, the lower B in radio loud sources could be due a lower electron T in RL than in RQ, which could be, according to Figure 12, in turn associated with a lower U and a larger distance.

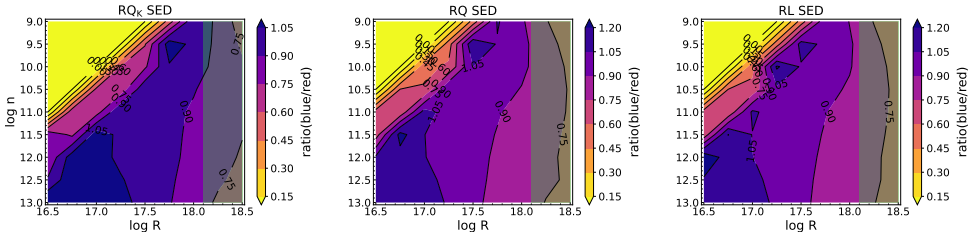

Figure 12. Results of CLOUDY simulations: the three panels yield the ratio $R_{\rm FeII}$ B to $R_{\rm FeII}$R (in practice B/R) as a function of density and BLR radius, for the RQ Korista et al. [89] (**leftmost**), the RQ Laor et al. [104] (**middle**) and RL SED (**rightmost**).

6.3. γ-Detected NLSy1s

The photoionization calculations performed with the parameters appropriate to model 1H 0323+342 (Figure 13, repeated in Appendix A for the restricted range as Figure A4) reveal that it is not possible to achieve $R_{\rm FeII} \sim 1$ with the SED shown in Figure 9. This raises an important issue about the FeII emission in these jetted sources. A change in SED within the limit of Population B, such as the one provided by Korista et al. [89] is likely not enough to explain the increase in FeII. This leaves several other possibilities to account for this intrinsic difference between jetted and non-jetted sources. They can be loosely grouped in "evolutionary" (chemical evolution of the host and of the

circumnuclear regions, in turn related to the host morphology), and "intrinsic" (density, column density, ionization degree, covering fraction of the line emitting gas). The host morphologies of RL and RQ are systematically different, and recent work has validated the long-held paradigm that RL are hosted in earlier morphological types than RQ [105,106]. This result might not be applicable to NLSy1s, and especially to the ones that are moderate-to-strong FeII emitters. Basically all of the recent studies on the host of jetted RL NLSy1s [107–109] showed that they are in late-type hosts. Merging is instead rather common, and it may constitute the biggest difference with respect to RQ NLSy1. In particular, Olguín-Iglesias et al. [109] clearly pointed out on a rather large sample that disk galaxies dominate among jetted NLSy1s.

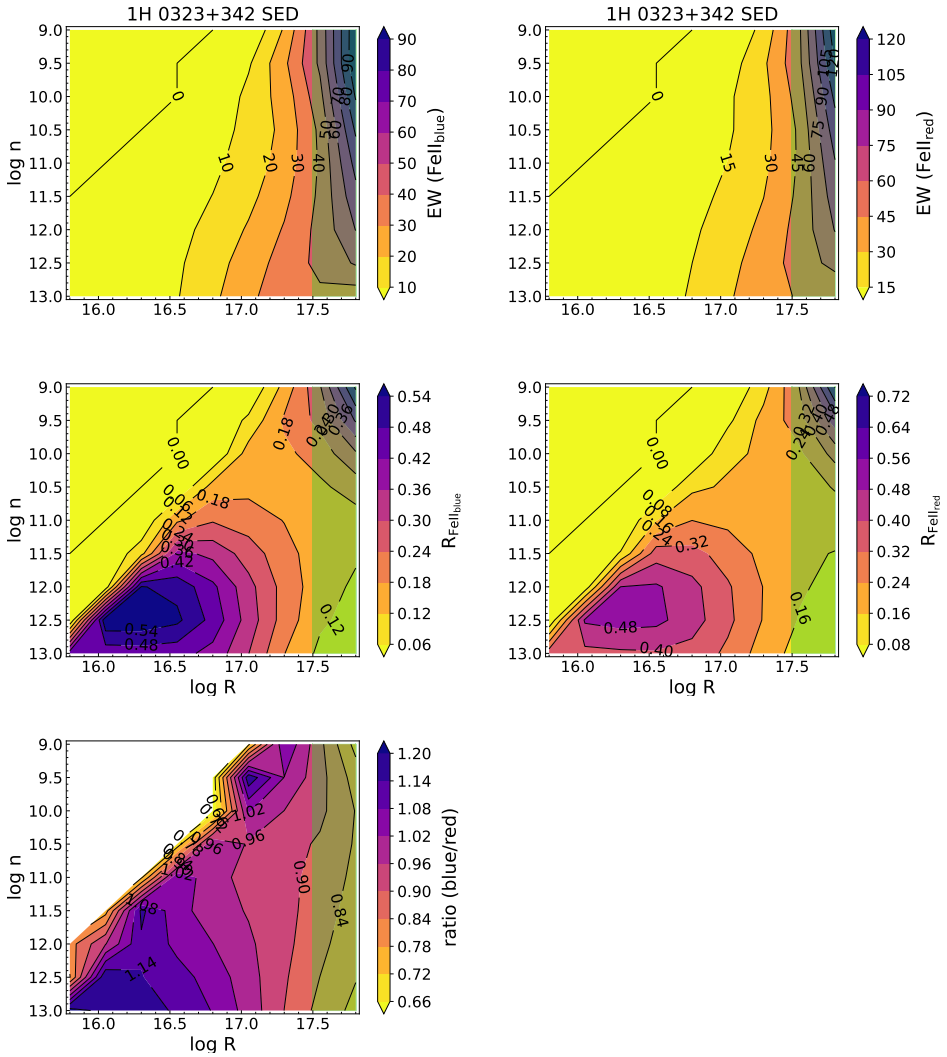

Figure 13. Results of CLOUDY simulations for the 1H 0323+342 SED: the two top panel yields the equivalent width of FeIIλ4570 and the two middle panels R_{FeII} for the blue and red blends, as a function of density and BLR radius. The bottom panel shows the ratio of the blue and red FeII emission.

The visual inspection of almost all known RL NLSy1s suggests that they never reach the extreme R_{FeII} value obtained by RQ sources. This impression—even if consistent with the difference found for weak FeII emitters—should be validated by a systematic study that goes beyond the scope of the present paper. Enrichment in chemical composition appears a likely possibility, as the strongest FeII emitters are also believed to have the highest metal content [96,110–112]. Photoionization analyses indicate that significant FeII

emission is associated with super-solar metallicity, in addition to high density and high column density [30,31], although a complete observational analysis with matching $R_{\rm FeII}$ and UV line diagnostics for metallicity and physical parameters estimates along the main sequence is still lacking.

7. Summary and Conclusions

This work presented an analysis of the FeII emission in the spectral bins along the main sequence where both RQ and RL coexist (A1, B1) with measurable FeII strength, and a comparison between the emission of RQ and RL composite template, along with the analysis of three RL sources found to have a stronger FeII emission. The main results can be summarized as follows:

- the template based on the I Zw 1 spectrum works equally well for RQ and RL objects. Deviation in $R_{\rm FeII}$ and equivalent width measurements due to differences between the template and the observed spectra have been found to be $\delta R_{\rm FeII} \lesssim 0.03$, and $\delta W \lesssim$ a few Å. In particular, no correction is needed for the placement of RL in the MS built from RQ-dominated samples;
- The RL SED of Laor et al. [88] can account for the modest emission in RL sources, for conditions that are very likely in Population B objects [31];
- Somewhat surprisingly, SED differences between RQ and RL cannot account for the stronger FeII emission in RQ[9]. We suggest that other factors related to the evolutionary pattern of the circumnuclear regions of the active nucleus should be investigated;
- Last, the SED shape does not seem so important in determining the optical FeII prominence with respect to Hβ for such sources with intermediate Eddington ratios ($\sim$0.1), as the change from the Laor et al. [88] to the Korista et al. [89] SED produces no significant change in $R_{\rm FeII}$, even if the number of ionizing photons is increased by a factor $\approx$3. We remark that, for sources at higher Eddington ratios, this might be different, as has been tested and shown in Panda et al. [31]. Those authors found that the SED shape matters for pushing the $R_{\rm FeII}$ higher, especially when the contribution from a soft-X-ray excess is accounted for.
- The ratio between the B and the R blend is found to be $\approx$ 0.9–1.0 and to be consistent with the predictions of the photoionization computation. A slightly lower value ($\approx$0.7) might be possible for the B1 RL composites. However, the measurement is excruciatingly difficult, considering the uncertain influence of the HeIIλ4686 emission that is known to be very strong in cases where FeII is negligible (e.g., [113]), and of several other factors that should play a lesser role. More importantly, the B/R value around $\approx$ 1 is found also in higher Eddington ratio sources which are stronger FeII emitters such as the 3 γ-detected NLSy1s considered in this study, all with Eddington ratio $\approx$ 0.5, typical of Population A quasars. Since $R_{\rm FeII}$ is correlated with Eddington ratio [114,115], and the B/R is apparently independent from $R_{\rm FeII}$, a lower B/R might be a genuine radio loudness effect or, perhaps more likely, an effect dependent on other RQ/RL sample differences.

In summary, we find that the FeII emission is stable, and we confirm that a solid template based on I Zw 1 provides an accurate representation of the optical FeII emission in the spectral region of Hβ within the limit of precision allowed by moderate dispersion spectroscopy.

Author Contributions: P.M. wrote most of the paper; M.B. contributed the NLSy1 spectra and the SED, and wrote a part of the text; S.P. performed the simulations and made the plots; E.B. contributed with suggestions and critical reading. All authors have read and agreed to the published version of the manuscript.

Funding: S.P. would like to acknowledge the financial support by the Polish Funding Agency National Science Centre, project 2017/26/A/ST9/00756 (MAESTRO 9), and from CNPq Fellowship (164753/2020-6). E.B. acknowledge the support of Serbian Ministry of Education, Science and Technological Development, through the contract number 451-03-68/2020-14/200002. Funding for the Sloan Digital Sky Survey has been provided by the Alfred P. Sloan Foundation, and the U.S. Department of Energy Office of Science.

Institutional Review Board Statement: Not applicable.

Informed Consent Statement: Not applicable.

Data Availability Statement: Data could be made in part available upon request.

Acknowledgments: Based on observations made with ESO Telescopes at the La Silla Paranal Observatory under program ID 096.B-0256. This work is partially based on observations made with the Galileo 1.22 m telescope of the Asiago Astrophysical Observatory operated by the Department of Physics and Astronomy "G. Galilei" of the University of Padova.The SDSS web site is http://www.sdss.org (accessed on 30 November 2021). SDSS-III is managed by the Astrophysical Research Consortium for the Participating Institutions of the SDSS-III Collaboration including the University of Arizona, the Brazilian Participation Group, Brookhaven National Laboratory, Carnegie Mellon University, University of Florida, the French Participation Group, the German Participation Group, Harvard University, the Instituto de Astrofisica de Canarias, the Michigan State/Notre Dame/JINA Participation Group, Johns Hopkins University, Lawrence Berkeley National Laboratory, Max Planck Institute for Astrophysics, Max Planck Institute for Extraterrestrial Physics, New Mexico State University, University of Portsmouth, Princeton University, the Spanish Participation Group, University of Tokyo, University of Utah, Vanderbilt University, University of Virginia, University of Washington, and Yale University.

Conflicts of Interest: The authors declare no conflict of interest.

Abbreviations

The following abbreviations are used in this manuscript:

AGN	Active Galactic Nucleus
BLR	Broad Line Region
CD	Core dominated
FR-I	Fanaroff-Riley I
FR-II	Fanaroff-Riley II
FWHM	Full Width Half-Maximum
MS	Main Sequence
NLSy1	Narrow-Line Seyfert 1
RL	Radio loud
RQ	Radio quiet
SDSS	Sloan Digital Sky Survey
SED	Spectral energy distribution
S/N	Signal-to-noise ratio

Appendix A. Restricted Range

The Appendix shows the results of the CLOUDY simulations in the case of the restricted ranges 4500–4590 Å and 5200–5300 Å ($\tilde{B}$ and $\tilde{R}$ through the paper).

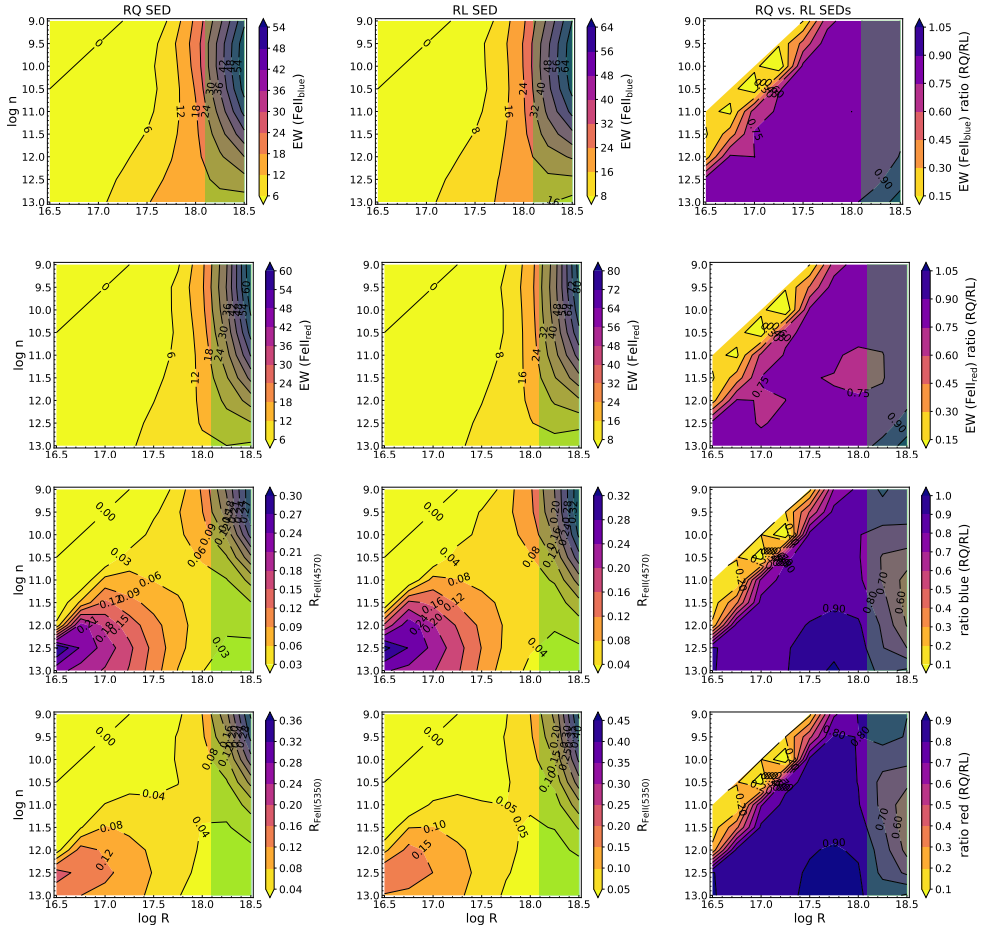

Figure A1. Results of CLOUDY simulations. First two rows: W(FeIIλ4570) for RQ and RL (i.e., computed for the same physical parameters but with the two different SEDs of Laor et al. [88]) and their ratios; third and fourth row from top: $R_{\rm FeII}$, for RQ and RL and their ratios. Last four rows: same, for the red (R) FeII blend peaked at λ 5312 Å.

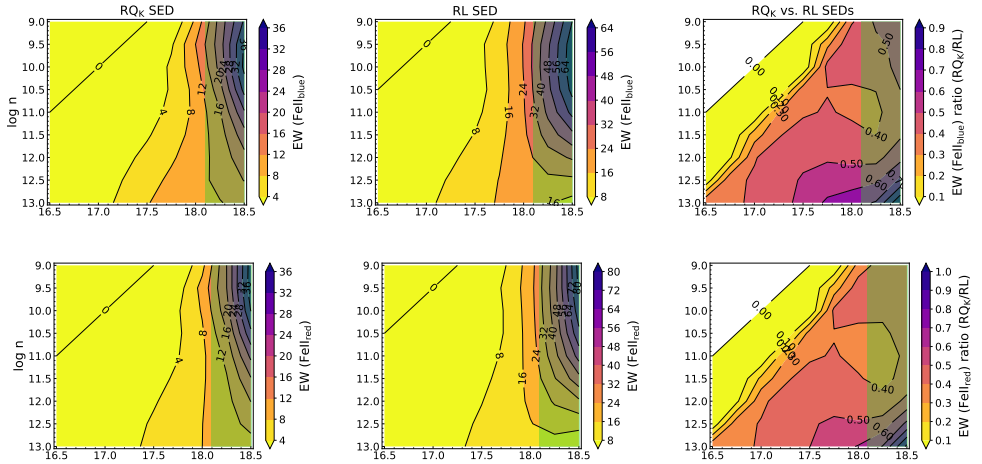

Figure A2. *Cont.*

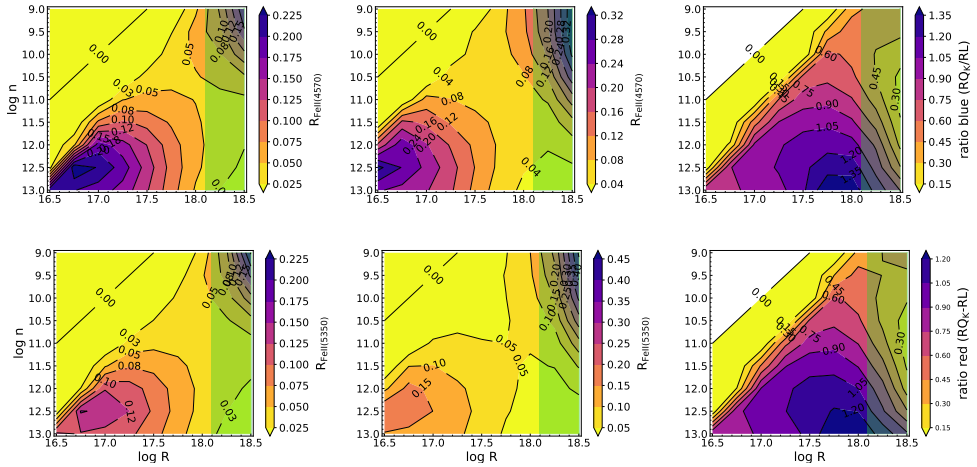

Figure A2. Results of CLOUDY simulations, same as in Figure 12 but for the RQ SED of Korista et al. [89].

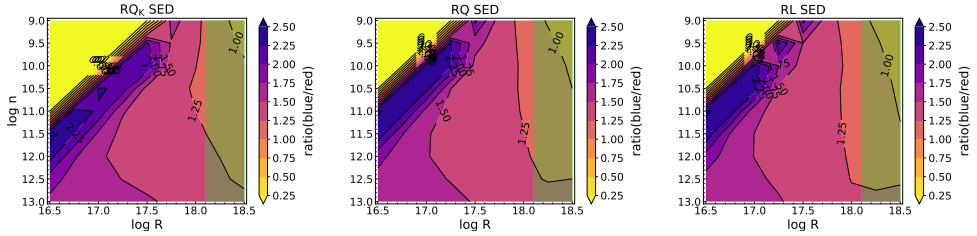

Figure A3. Results of CLOUDY simulations: the three panels yield the ratio $R_{\rm FeII}$ $\tilde{\rm B}$ to $R_{\rm FeII}\tilde{\rm R}$ (in practice $\tilde{\rm B}/\tilde{\rm R}$) as a function of density and BLR radius, for the RQ Korista et al. [89] (**leftmost**), the RQ Laor et al. [104] (**middle**) and RL SED (**rightmost**).

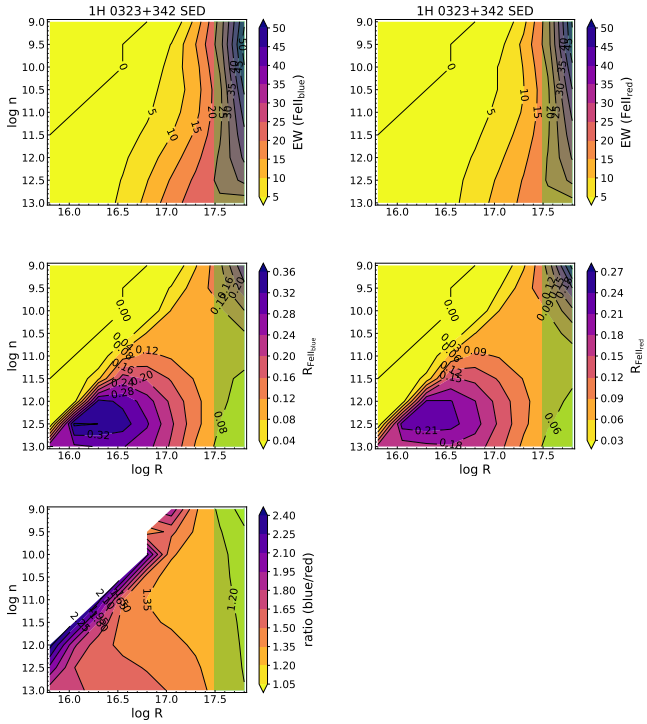

Figure A4. Results of CLOUDY simulations for the 1H0323+342 SED: the two top panel yields the equivalent width of FeIIλ4570 and the two middle panels $R_{\rm FeII}$ for the blue and red blends, as a function of density and BLR radius. The bottom panel shows the ratio of the blue and red FeII emission.

Notes

[1] For an introduction to AGN spectra and the interpretation of their spectra in physical terms, see for example, [1–3], and references therein.

[2] Type-2 AGN do not show broad permitted lines in natural light; they are believed to be mostly obscured type-1 and will not be further considered here because they lack the diagnostics offered by the broad lines measurements.

[3] We consider here only powerful jetted radio sources with radio-to-optical specific flux ratio $R \gtrsim 80$ as radio loud (RL).

[4] Both FR-I and FR-II sources are characterized by extended radio emission. FR-Is, however, show lower radio surface brightness toward the outer extremities of the lobes, at variance with FR-II sources that are often described as "edge brightened". According to the unification schemes [60], both classes are observed at relatively high inclination. Their optical spectra can be of both type 1 and type 2 AGN.

[5] http://servo.aob.rs/FeII_AGN/ (accessed on 30 November 2021).

[6] http://servo.aob.rs/FeII_AGN/uploads.php (accessed on 30 November 2021).

[7] I Zw 1 is however not a very extreme object: the most extreme accretors show spectra similar to the one of PHL 1092 [86].

[8] https://tools.ssdc.asi.it/SED/ (accessed on 30 November 2021).

[9] Note that the equivalent width is increased, as shown in Figures 11 and A2 but, since there is a corresponding increase in Hβ, the $R_{\rm FeII}$ is left unaffected.

References

1. Netzer, H. AGN emission lines. In *Active Galactic Nuclei*; Blandford, R.D., Netzer, H., Woltjer, L., Courvoisier, T.J.-L., Mayor, M., Eds.; Springer: Berlin, Germany, 1990; pp. 57–160.
2. Peterson, B.M. *An Introduction to Active Galactic Nuclei*; Cambridge University Press: Cambridge, UK, 1997.
3. Osterbrock, D.E.; Ferland, G.J. *Astrophysics of Gaseous Nebulae and Active Galactic Nuclei*; University Science Books: Mill Valley, CA, USA, 2006.
4. Boroson, T.A.; Green, R.F. The Emission-Line Properties of Low-Redshift Quasi-stellar Objects. *Astrophys. J. Suppl. Ser.* **1992**, *80*, 109 . [CrossRef]
5. Sulentic, J.W.; Marziani, P.; Dultzin-Hacyan, D. Phenomenology of Broad Emission Lines in Active Galactic Nuclei. *Annu. Rev. Astron. Astrophys.* **2000**, *38*, 521–571. [CrossRef]
6. Marziani, P.; Sulentic, J.W.; Zwitter, T.; Dultzin-Hacyan, D.; Calvani, M. Searching for the Physical Drivers of the Eigenvector 1 Correlation Space. *Astrophys. J.* **2001**, *558*, 553–560. [CrossRef]
7. Shen, Y.; Ho, L.C. The diversity of quasars unified by accretion and orientation. *Nature* **2014**, *513*, 210–213. [CrossRef] [PubMed]
8. Gaskell, C.M. Galactic mergers, starburst galaxies, quasar activity and massive binary black holes. *Nature* **1985**, *315*, 386. [CrossRef]
9. Sulentic, J.; Marziani, P. Quasars in the 4D Eigenvector 1 Context: A stroll down memory lane. *Front. Astron. Space Sci.* **2015**, *2*, 6. [CrossRef]
10. Sulentic, J.W.; Marziani, P.; Zamanov, R.; Bachev, R.; Calvani, M.; Dultzin-Hacyan, D. Average Quasar Spectra in the Context of Eigenvector 1. *Astrophys. J. Lett.* **2002**, *566*, L71–L75. [CrossRef]
11. Sulentic, J.W.; Zamfir, S.; Marziani, P.; Dultzin, D. Our Search for an H-R Diagram of Quasars. In *Revista Mexicana de Astronomia y Astrofisica Conference Series*; 2008; Volume 32, pp. 51–58. Available online: https://arxiv.org/abs/0709.2499v1 (accessed on 30 November 2021).
12. Fraix-Burnet, D.; Marziani, P.; D'Onofrio, M.; Dultzin, D. The Phylogeny of Quasars and the Ontogeny of Their Central Black Holes. *Front. Astron. Space Sci.* **2017**, *4*, 1. [CrossRef]
13. Leighly, K.M.; Moore, J.R. Hubble Space Telescope STIS Ultraviolet Spectral Evidence of Outflow in Extreme Narrow-Line Seyfert 1 Galaxies. I. Data and Analysis. *Astrophys. J.* **2004**, *611*, 107–124. [CrossRef]
14. Richards, G.T.; Kruczek, N.E.; Gallagher, S.C.; Hall, P.B.; Hewett, P.C.; Leighly, K.M.; Deo, R.P.; Kratzer, R.M.; Shen, Y. Unification of Luminous Type 1 Quasars through C IV Emission. *Astron. J.* **2011**, *141*, 167. [CrossRef]
15. Coatman, L.; Hewett, P.C.; Banerji, M.; Richards, G.T. C iv emission-line properties and systematic trends in quasar black hole mass estimates. *Mon. Not. R. Astron. Soc.* **2016**, *461*, 647–665. [CrossRef]
16. Marziani, P.; Martínez Carballo, M.A.; Sulentic, J.W.; Del Olmo, A.; Stirpe, G.M.; Dultzin, D. The most powerful quasar outflows as revealed by the Civ λ1549 resonance line. *Astrophys. Space Sci.* **2016**, *361*, 29. [CrossRef]
17. Sulentic, J.W.; del Olmo, A.; Marziani, P.; Martínez-Carballo, M.A.; D'Onofrio, M.; Dultzin, D.; Perea, J.; Martínez-Aldama, M.L.; Negrete, C.A.; Stirpe, G.M.; et al. What does CIVλ1549 tell us about the physical driver of the Eigenvector quasar sequence? *Astron. Astrophys.* **2017**, *608*, A122. [CrossRef]
18. Vietri, G.; Piconcelli, E.; Bischetti, M.; Duras, F.; Martocchia, S.; Bongiorno, A.; Marconi, A.; Zappacosta, L.; Bisogni, S.; Bruni, G.; et al. The WISSH quasars project. IV. Broad line region versus kiloparsec-scale winds. *Astron. Astrophys.* **2018**, *617*, A81. [CrossRef]
19. Marziani, P.; Zamanov, R.K.; Sulentic, J.W.; Calvani, M. Searching for the physical drivers of eigenvector 1: Influence of black hole mass and Eddington ratio. *Mon. Not. R. Astron. Soc.* **2003**, *345*, 1133–1144. [CrossRef]

20. Marziani, P.; Sulentic, J.W.; Stirpe, G.M.; Zamfir, S.; Calvani, M. VLT/ISAAC spectra of the Hβ region in intermediate-redshift quasars. III. Hβ broad-line profile analysis and inferences about BLR structure. *Astron. Astrophys.* **2009**, *495*, 83–112.[CrossRef]
21. Wang, J.M.; Du, P.; Brotherton, M.S.; Hu, C.; Songsheng, Y.Y.; Li, Y.R.; Shi, Y.; Zhang, Z.X. Tidally disrupted dusty clumps as the origin of broad emission lines in active galactic nuclei. *Nat. Astron.* **2017**, *1*, 775–783. [CrossRef]
22. Corbin, M.R. QSO Broad Emission Line Asymmetries: Evidence of Gravitational Redshift? *Astrophys. J.* **1995**, *447*, 496. [CrossRef]
23. Popovic, L.C.; Vince, I.; Atanackovic-Vukmanovic, O.; Kubicela, A. Contribution of gravitational redshift to spectral line profiles of Seyfert galaxies and quasars. *Astron. Astrophys.* **1995**, *293*, 309–314.
24. Zheng, W.; Sulentic, J.W. Internal Redshift Difference and Central Mass in QSOs. *Astrophys. J.* **1990**, *350*, 512. [CrossRef]
25. Bon, N.; Bon, E.; Marziani, P.; Jovanović, P. Gravitational redshift of emission lines in the AGN spectra. *Astrophys. Space Sci.* **2015**, *360*, 7. [CrossRef]
26. Punsly, B.; Marziani, P.; Berton, M.; Kharb, P. The Extreme Red Excess in Blazar Ultraviolet Broad Emission Lines. *Astrophys. J.* **2020**, *903*, 44. [CrossRef]
27. Marinello, A.O.M.; Rodriguez-Ardila, A.; Garcia-Rissmann, A.; Sigut, T.A.A.; Pradhan, A.K. The FeII emission in active galactic nuclei: Excitation mechanisms and location of the emitting region. *Astrophys. J.* **2016**, *820*, 116. [CrossRef]
28. Marziani, P.; Sulentic, J.W.; Plauchu-Frayn, I.; del Olmo, A. Is Mg II 2800 a Reliable Virial Broadening Estimator for Quasars? *Astron. Astrophys.* **2013**, *555*, A89. [CrossRef]
29. Marziani, P.; Sulentic, J.W.; Negrete, C.A.; Dultzin, D.; Zamfir, S.; Bachev, R. Broad-line region physical conditions along the quasar eigenvector 1 sequence. *Mon. Not. R. Astron. Soc.* **2010**, *409*, 1033–1048. [CrossRef]
30. Panda, S.; Czerny, B.; Adhikari, T.P.; Hryniewicz, K.; Wildy, C.; Kuraszkiewicz, J.; Śniegowska, M. Modeling of the Quasar Main Sequence in the Optical Plane. *Astrophys. J.* **2018**, *866*, 115. [CrossRef]
31. Panda, S.; Marziani, P.; Czerny, B. The Quasar Main Sequence Explained by the Combination of Eddington Ratio, Metallicity, and Orientation. *Astrophys. J.* **2019**, *882*, 79. [CrossRef]
32. Steiner, J.E. A spectrophotometric classification of low-redshift quasars and active galactic nuclei. *Astrophys. J.* **1981**, *250*, 469–477. [CrossRef]
33. Boller, T.; Brandt, W.N.; Fink, H. Soft X-ray properties of narrow-line Seyfert 1 galaxies. *Astron. Astrophys.* **1996**, *305*, 53.
34. Wang, T.; Brinkmann, W.; Bergeron, J. X-ray properties of active galactic nuclei with optical FeII emission. *Astron. Astrophys.* **1996**, *309*, 81–96.
35. Sulentic, J.W.; Marziani, P.; Zwitter, T.; Dultzin-Hacyan, D.; Calvani, M. The Demise of the Classical Broad-Line Region in the Luminous Quasar PG 1416-129. *Astrophys. J. Lett.* **2000**, *545*, L15–L18. [CrossRef]
36. Grupe, D.; Thomas, H.C.; Beuermann, K. X-ray variability in a complete sample of Soft X-ray selected AGN. *Astron. Astrophys.* **2001**, *367*, 470–486.[CrossRef]
37. Panda, S.; Marziani, P.; Czerny, B. FeII emission in NLS1s—Originating from denser regions with higher abundances? *IAU Symp.* **2021**, *356*, 77–81. [CrossRef]
38. Panda, S.; Maλek, K.; Śniegowska, M.; Czerny, B. Strong FeII emission in NLS1s: An unsolved mystery. In *Panchromatic Modelling with Next Generation Facilities*; Boquien, M., Lusso, E., Gruppioni, C., Tissera, P., Eds.; Cambridge University Press: Cambridge, UK, 2020; Volume 341, pp. 297–298. [CrossRef]
39. Panda, S.; Marziani, P.; Czerny, B. FeII strength in NLS1s—Dependence on the viewing angle and FWHM(Hβ). *IAU Symp.* **2021**, *356*, 332–334. [CrossRef]
40. Joly, M.; Véron-Cetty, M.; Véron, P. Fe II emission in AGN. In *Revista Mexicana de Astronomia y Astrofisica Conference Series*; 2008; Volume 32, pp. 59–61. Available online: https://www.redalyc.org/pdf/571/57103222.pdf (accessed on 30 November 2021).
41. Barth, A.J.; Pancoast, A.; Bennert, V.N.; Brewer, B.J.; Canalizo, G.; Filippenko, A.V.; Gates, E.L.; Greene, J.E.; Li, W.; Malkan, M.A.; et al. The Lick AGN Monitoring Project 2011: Fe II Reverberation from the Outer Broad-line Region. *Astrophys. J.* **2013**, *769*, 128. [CrossRef]
42. Du, P.; Zhang, Z.X.; Wang, K.; Huang, Y.K.; Zhang, Y.; Lu, K.X.; Hu, C.; Li, Y.R.; Bai, J.M.; Bian, W.H.; et al. Supermassive Black Holes with High Accretion Rates in Active Galactic Nuclei. IX. 10 New Observations of Reverberation Mapping and Shortened Hβ Lags. *Astrophys. J.* **2018**, *856*, 6. [CrossRef]
43. Sulentic, J.W.; Zamfir, S.; Marziani, P.; Bachev, R.; Calvani, M.; Dultzin-Hacyan, D. Radio-loud Active Galactic Nuclei in the Context of the Eigenvector 1 Parameter Space. *Astrophys. J. Lett.* **2003**, *597*, L17–L20. [CrossRef]
44. Zamfir, S.; Sulentic, J.W.; Marziani, P. New insights on the QSO radio-loud/radio-quiet dichotomy: SDSS spectra in the context of the 4D eigenvector1 parameter space. *Mon. Not. R. Astron. Soc.* **2008**, *387*, 856–870. [CrossRef]
45. Bonzini, M.; Mainieri, V.; Padovani, P.; Andreani, P.; Berta, S.; Bethermin, M.; Lutz, D.; Rodighiero, G.; Rosario, D.; Tozzi, P.; et al. Star formation properties of sub-mJy radio sources. *Mon. Not. R. Astron. Soc.* **2015**, *453*, 1079–1094. [CrossRef]
46. Caccianiga, A.; Antón, S.; Ballo, L.; Foschini, L.; Maccacaro, T.; Della Ceca, R.; Severgnini, P.; Marchã, M.J.; Mateos, S.; Sani, E. WISE colours and star formation in the host galaxies of radio-loud narrow-line Seyfert 1. *Mon. Not. R. Astron. Soc.* **2015**, *451*, 1795–1805. [CrossRef]
47. Ganci, V.; Marziani, P.; D'Onofrio, M.; del Olmo, A.; Bon, E.; Bon, N.; Negrete, C.A. Radio loudness along the quasar main sequence. *Astron. Astrophys.* **2019**, *630*, A110. [CrossRef]
48. Osterbrock, D.E. Spectrophotometry of Seyfert 1 galaxies. *Astrophys. J.* **1977**, *215*, 733–745. [CrossRef]

49. Miley, G.K.; Miller, J.S. Relations between the emission spectra and radio structures of quasars. *Astrophys. J.* **1979**, *228*, L55–L58. [CrossRef]
50. Phillips, M.M. Permitted fe II Emission in Seyfert 1 Galaxies and QSOs I. Observations. *Astrophys. J. Suppl. Ser.* **1978**, *38*, 187. [CrossRef]
51. Pradhan, A.K.; Nahar, S.N. *Atomic Astrophysics and Spectroscopy*; Cambridge University Press: Cambridge, UK, 2015.
52. Verner, E.M.; Verner, D.A.; Korista, K.T.; Ferguson, J.W.; Hamann, F.; Ferland, G.J. Numerical Simulations of Fe II Emission Spectra. *Astrophys. J. Suppl. Ser.* **1999**, *120*, 101–112. [CrossRef]
53. Verner, E.; Bruhweiler, F.; Verner, D.; Johansson, S.; Kallman, T.; Gull, T. Fe II Diagnostic Tools for Quasars. *Astrophys. J.* **2004**, *611*, 780–785. [CrossRef]
54. Sigut, T.A.A.; Pradhan, A.K. Ly alpha Flourescent Excitation of Fe II in Active Galactic Nuclei. *Astrophys. J. Lett.* **1998**, *499*, L139. [CrossRef]
55. Sigut, T.A.A.; Pradhan, A.K. Predicted Fe II Emission-Line Strengths from Active Galactic Nuclei. *Astrophys. J. Suppl. Ser.* **2003**, *145*, 15–37. [CrossRef]
56. Phillips, M.M. Permitted Fe II emission in Seyfert 1 galaxies and QSOs. II—The excitation mechanism. *Astrophys. J.* **1978**, *226*, 736–752. [CrossRef]
57. Marziani, P.; Sulentic, J.W.; Plauchu-Frayn, I.; del Olmo, A. Low-Ionization Outflows in High Eddington Ratio Quasars. *Astrophys. J.* **2013**, *764*, 150. [CrossRef]
58. de Young, D.S. *The Physics of Extragalactic Radio Sources*; University of Chicago Press: Chicago, IL, USA, 2002.
59. Kembhavi, A.K.; Narlikar, J.V. *Quasars and Active Galactic Nuclei: An Introduction*; Cambridge University Press: Cambridge, UK, 1999.
60. Urry, C.M.; Padovani, P. Unified Schemes for Radio-Loud Active Galactic Nuclei. *Publ. Astron. Soc. Pac.* **1995**, *107*, 803. [CrossRef]
61. Komossa, S.; Voges, W.; Xu, D.; Mathur, S.; Adorf, H.M.; Lemson, G.; Duschl, W.J.; Grupe, D. Radio-loud Narrow-Line Type 1 Quasars. *Astron. J.* **2006**, *132*, 531–545. [CrossRef]
62. Zhou, H.; Wang, T.; Yuan, W.; Lu, H.; Dong, X.; Wang, J.; Lu, Y. A Comprehensive Study of 2000 Narrow Line Seyfert 1 Galaxies from the Sloan Digital Sky Survey. I. The Sample. *Astrophys. J. Suppl. Ser.* **2006**, *166*, 128–153. [CrossRef]
63. Antón, S.; Browne, I.W.A.; Marchã, M.J. The colour of the narrow line Sy1-blazar 0324+3410. *Astron. Astrophys.* **2008**, *490*, 583–587. [CrossRef]
64. Kynoch, D.; Landt, H.; Ward, M.J.; Done, C.; Gardner, E.; Boisson, C.; Arrieta-Lobo, M.; Zech, A.; Steenbrugge, K.; Pereira Santaella, M. The relativistic jet of the γ-ray emitting narrow-line Seyfert 1 galaxy 1H 0323+342. *Mon. Not. R. Astron. Soc.* **2018**, *475*, 404–423. [CrossRef]
65. Abdo, A.A.; Ackermann, M.; Ajello, M.; Atwood, W.B.; Axelsson, M.; Baldini, L.; Ballet, J.; Band, D.L.; Barbiellini, G.; Bastieri, D.; et al. Fermi/Large Area Telescope Bright Gamma-Ray Source List. *Astrophys. J. Suppl. Ser.* **2009**, *183*, 46–66. [CrossRef]
66. Ackermann, M.; Ajello, M.; Atwood, W.B.; Baldini, L.; Ballet, J.; Barbiellini, G.; Bastieri, D.; Becerra Gonzalez, J.; Bellazzini, R.; Bissaldi, E.; et al. The Third Catalog of Active Galactic Nuclei Detected by the Fermi Large Area Telescope. *Astrophys. J.* **2015**, *810*, 14. [CrossRef]
67. Peacock, J.A.; Wall, J.V. Bright extragalactic radio sources at 2.7 GHz- II. Observations with the Cambridge 5-km telescope. *Mon. Not. R. Astron. Soc.* **1982**, *198*, 843–860. [CrossRef]
68. Berton, M.; Foschini, L.; Caccianiga, A.; Ciroi, S.; Congiu, E.; Cracco, V.; Frezzato, M.; La Mura, G.; Rafanelli, P. An orientation-based unification of young jetted active galactic nuclei: The case of 3C 286. *Front. Astron. Space Sci.* **2017**, *4*, 8. [CrossRef]
69. Yao, S.; Komossa, S. Spectroscopic classification, variability, and SED of the Fermi-detected CSS 3C 286: The radio-loudest NLS1 galaxy? *Mon. Not. R. Astron. Soc.* **2021**, *501*, 1384–1393. [CrossRef]
70. Oshlack, A.Y.K.N.; Webster, R.L.; Whiting, M.T. A Very Radio Loud Narrow-Line Seyfert 1: PKS 2004-447. *Astrophys. J.* **2001**, *558*, 578–582. [CrossRef]
71. Gallo, L.C.; Edwards, P.G.; Ferrero, E.; Kataoka, J.; Lewis, D.R.; Ellingsen, S.P.; Misanovic, Z.; Welsh, W.F.; Whiting, M.; Boller, T.; et al. The spectral energy distribution of PKS 2004-447: A compact steep-spectrum source and possible radio-loud narrow-line Seyfert 1 galaxy. *Mon. Not. R. Astron. Soc.* **2006**, *370*, 245–254. [CrossRef]
72. Berton, M.; Peluso, G.; Marziani, P.; Komossa, S.; Foschini, L.; Ciroi, S.; Chen, S.; Congiu, E.; Gallo, L.C.; Björklund, I.; et al. Hunting for the nature of the enigmatic narrow-line Seyfert 1 galaxy PKS 2004-447. *arXiv* **2021**, arXiv:2106.12536.
73. Foschini, L.; Berton, M.; Caccianiga, A.; Ciroi, S.; Cracco, V.; Peterson, B.M.; Angelakis, E.; Braito, V.; Fuhrmann, L.; Gallo, L.; et al. Properties of flat-spectrum radio-loud narrow-line Seyfert 1 galaxies. *Astron. Astrophys.* **2015**, *575*, A13. [CrossRef]
74. Sulentic, J.W.; Martínez-Carballo, M.A.; Marziani, P.; del Olmo, A.; Stirpe, G.M.; Zamfir, S.; Plauchu-Frayn, I. 3C 57 as an atypical radio-loud quasar: Implications for the radio-loud/radio-quiet dichotomy. *Mon. Not. R. Astron. Soc.* **2015**, *450*, 1916–1925. [CrossRef]
75. Negrete, C.A.; Dultzin, D.; Marziani, P.; Esparza, D.; Sulentic, J.W.; del Olmo, A.; Martínez-Aldama, M.L.; García López, A.; D'Onofrio, M.; Bon, N.; et al. Highly accreting quasars: The SDSS low-redshift catalog. *Astron. Astrophys.* **2018**, *620*, A118. [CrossRef]
76. Marziani, P.; del Olmo, A.; Martinez-Carballo, M.A.; Martinez-Aldama, M.L.; Stirpe, G.M.; Negrete, C.A.; Dultzin, D.; D' Onofrio, M.; Bon, E.; Bon, N. Black hole mass estimates in quasars—A comparative analysis of high- and low-ionisation lines. *arXiv* **2019**, arXiv:1905.00617.

77. Wolf, J.; Salvato, M.; Coffey, D.; Merloni, A.; Buchner, J.; Arcodia, R.; Baron, D.; Carrera, F.J.; Comparat, J.; Schneider, D.P.; et al. Exploring the diversity of Type 1 active galactic nuclei identified in SDSS-IV/SPIDERS. *Mon. Not. R. Astron. Soc.* **2020**, *492*, 3580–3601. [CrossRef]
78. Kovačević, J.; Popović, L.Č.; Dimitrijević, M.S. Analysis of Optical Fe II Emission in a Sample of Active Galactic Nucleus Spectra. *Astrophys. J. Suppl. Ser.* **2010**, *189*, 15–36. [CrossRef]
79. Kovačević-Dojčinović, J.; Popović, L.Č. The Connections Between the UV and Optical Fe ii Emission Lines in Type 1 AGNs. *Astrophys. J. Suppl. Ser.* **2015**, *221*, 35. [CrossRef]
80. Marziani, P.; Sulentic, J.W.; Dultzin-Hacyan, D.; Calvani, M.; Moles, M. Comparative Analysis of the High- and Low-Ionization Lines in the Broad-Line Region of Active Galactic Nuclei. *Astrophys. J. Suppl. Ser.* **1996**, *104*, 37. [CrossRef]
81. Punsly, B. The Redshifted Excess in Quasar C IV Broad Emission Lines. *Astrophys. J.* **2010**, *713*, 232–238. [CrossRef]
82. Moore, C.E. A Multiplet Table of Astrophysical Interest. Revised Edition. Part I—Table of Multiplets. *Contrib. Princet. Univ. Obs.* **1945**, *20*, 1–110.
83. Kriss, G. Fitting Models to UV and Optical Spectral Data. *Astron. Data Anal. Softw. Syst. III* **1994**, *61*, 437.
84. Gaskell, C.M. The case for cases B and C: Intrinsic hydrogen line ratios of the broad-line region of active galactic nuclei, reddenings, and accretion disc sizes. *Mon. Not. R. Astron. Soc.* **2017**, *467*, 226–238. [CrossRef]
85. Baskin, A.; Laor, A. Dust inflated accretion disc as the origin of the broad line region in active galactic nuclei. *Mon. Not. R. Astron. Soc.* **2018**, *474*, 1970–1994. [CrossRef]
86. Marinello, M.; Overzier, R.A.; Röttgering, H.J.A.; Kurk, J.D.; De Breuck, C.; Vernet, J.; Wylezalek, D.; Stern, D.; Duncan, K.J.; Hatch, N.; et al. VLT/SINFONI study of black hole growth in high-redshift radio-loud quasars from the CARLA survey. *Mon. Not. R. Astron. Soc.* **2020**, *492*, 1991–2016. [CrossRef]
87. Davidson, K.; Netzer, H. The emission lines of quasars and similar objects. *Rev. Mod. Phys.* **1979**, *51*, 715–766. [CrossRef]
88. Laor, A.; Fiore, F.; Elvis, M.; Wilkes, B.J.; McDowell, J.C. The Soft X-Ray Properties of a Complete Sample of Optically Selected Quasars. II. Final Results. *Astrophys. J.* **1997**, *477*, 93. [CrossRef]
89. Korista, K.; Baldwin, J.; Ferland, G.; Verner, D. An Atlas of Computed Equivalent Widths of Quasar Broad Emission Lines. *Astrophys. J. Suppl. Ser.* **1997**, *108*, 401. [CrossRef]
90. Peterson, B.M.; Ferrarese, L.; Gilbert, K.M.; Kaspi, S.; Malkan, M.A.; Maoz, D.; Merritt, D.; Netzer, H.; Onken, C.A.; Pogge, R.W.; et al. Central Masses and Broad-Line Region Sizes of Active Galactic Nuclei. II. A Homogeneous Analysis of a Large Reverberation-Mapping Database. *Astrophys. J.* **2004**, *613*, 682–699. [CrossRef]
91. Peterson, B.M. Space Telescope and Optical Reverberation Mapping Project: A Leap Forward in Reverberation Mapping. In *IAU Symposium*; Cambridge University Press: Cambridge, UK, 2017; Volume 324, pp. 215–218. [CrossRef]
92. Collin-Souffrin, S.; Dumont, A.M. Emission spectra of weakly photoionized media in active nuclei of galaxies. *Astron. Astrophys.* **1989**, *213*, 29–48.
93. Collin, S.; Joly, M. The Fe II problem in NLS1s. *New Astron. Rev.* **2000**, *44*, 531–537. [CrossRef]
94. Matsuoka, Y.; Kawara, K.; Oyabu, S. Low-Ionization Emission Regions in Quasars: Gas Properties Probed with Broad O I and Ca II Lines. *Astrophys. J.* **2008**, *673*, 62–68. [CrossRef]
95. Martínez-Aldama, M.L.; Dultzin, D.; Marziani, P.; Sulentic, J.W.; Bressan, A.; Chen, Y.; Stirpe, G.M. O I and Ca II Observations in Intermediate Redshift Quasars. *Astrophys. J. Suppl. Ser.* **2015**, *217*, 3. [CrossRef]
96. Śniegowska, M.; Marziani, P.; Czerny, B.; Panda, S.; Martínez-Aldama, M.L.; del Olmo, A.; D'Onofrio, M. High Metal Content of Highly Accreting Quasars. *Astrophys. J.* **2021**, *910*, 115. [CrossRef]
97. Bentz, M.C.; Denney, K.D.; Grier, C.J.; Barth, A.J.; Peterson, B.M.; Vestergaard, M.; Bennert, V.N.; Canalizo, G.; De Rosa, G.; Filippenko, A.V.; et al. The Low-luminosity End of the Radius-Luminosity Relationship for Active Galactic Nuclei. *Astrophys. J.* **2013**, *767*, 149. [CrossRef]
98. Martínez-Aldama, M.L.; Czerny, B.; Kawka, D.; Karas, V.; Panda, S.; Zajaček, M.; Życki, P.T. Can Reverberation-measured Quasars Be Used for Cosmology? *Astrophys. J.* **2019**, *883*, 170. [CrossRef]
99. Du, P.; Wang, J.M. The Radius-Luminosity Relationship Depends on Optical Spectra in Active Galactic Nuclei. *Astrophys. J.* **2019**, *886*, 42. [CrossRef]
100. D'Onofrio, M.; Marziani, P.; Chiosi, C. Past, present and Future of the Scaling Relations of Galaxies and Active Galactic Nuclei. *arXiv* **2021**, arXiv:2109.06301.
101. Marziani, P.; Dultzin, D.; Sulentic, J.W.; Del Olmo, A.; Negrete, C.A.; Martinez-Aldama, M.L.; D'Onofrio, M.; Bon, E.; Bon, N.; Stirpe, G.M. A main sequence for quasars. *arXiv* **2018**, arXiv:180205575M.
102. Sulentic, J.W.; Marziani, P.; Del Olmo, A.; Zamfir, S. Balmer line shifts in quasars. *Astrophys. Space Sci.* **2016**, *361*, 55. [CrossRef]
103. Sulentic, J.W.; Bachev, R.; Marziani, P.; Negrete, C.A.; Dultzin, D. C IV λ1549 as an Eigenvector 1 Parameter for Active Galactic Nuclei. *Astrophys. J.* **2007**, *666*, 757–777. [CrossRef]
104. Laor, A.; Jannuzi, B.T.; Green, R.F.; Boroson, T.A. The Ultraviolet Properties of the Narrow-Line Quasar I ZW 1. *Astrophys. J.* **1997**, *489*, 656. [CrossRef]
105. Kozieλ-Wierzbowska, D.; Vale Asari, N.; Stasińska, G.; Sikora, M.; Goettems, E.I.; Wójtowicz, A. What Distinguishes the Host Galaxies of Radio-loud and Radio-quiet AGNs? *Astrophys. J.* **2017**, *846*, 42. [CrossRef]
106. Kozieλ-Wierzbowska, D.; Stasińska, G.; Vale Asari, N.; Sikora, M.; Goettems, E.; Wójtowicz, A. Pair-matching of radio-loud and radio-quiet AGNs. *Front. Astron. Space Sci.* **2017**, *4*, 39. [CrossRef]

107. Järvelä, E.; Lähteenmäki, A.; Berton, M. Near-infrared morphologies of the host galaxies of narrow-line Seyfert 1 galaxies. *Astron. Astrophys.* **2018**, *619*, A69. [CrossRef]
108. Berton, M.; Congiu, E.; Ciroi, S.; Komossa, S.; Frezzato, M.; Di Mille, F.; Antón, S.; Antonucci, R.; Caccianiga, A.; Coppi, P.; et al. The Interacting Late-type Host Galaxy of the Radio-loud Narrow-line Seyfert 1 IRAS 20181-2244. *Astron. J.* **2019**, *157*, 48. [CrossRef]
109. Olguín-Iglesias, A.; Kotilainen, J.; Chavushyan, V. The disc-like host galaxies of radio-loud narrow-line Seyfert 1s. *Mon. Not. R. Astron. Soc.* **2020**, *492*, 1450–1464. [CrossRef]
110. Shin, J.; Woo, J.H.; Nagao, T.; Kim, S.C. The Chemical Properties of Low-redshift QSOs. *Astrophys. J.* **2013**, *763*, 58. [CrossRef]
111. Sulentic, J.W.; Marziani, P.; del Olmo, A.; Dultzin, D.; Perea, J.; Alenka Negrete, C. GTC spectra of z $\approx$ 2.3 quasars: Comparison with local luminosity analogs. *Astron. Astrophys.* **2014**, *570*, A96. [CrossRef]
112. Nagao, T.; Maiolino, R.; Marconi, A. Gas metallicity in the narrow-line regions of high-redshift active galactic nuclei. *Astron. Astrophys.* **2006**, *447*, 863–876. [CrossRef]
113. Marziani, P.; Sulentic, J.W. Evidence for a very broad line region in PG 1138+222. *Astrophys. J.* **1993**, *409*, 612–616. [CrossRef]
114. Sun, J.; Shen, Y. Dissecting the Quasar Main Sequence: Insight from Host Galaxy Properties. *Astrophys. J. Lett.* **2015**, *804*, L15. [CrossRef]
115. Du, P.; Wang, J.M.; Hu, C.; Ho, L.C.; Li, Y.R.; Bai, J.M. The Fundamental Plane of the Broad-line Region in Active Galactic Nuclei. *Astrophys. J. Lett.* **2016**, *818*, L14. [CrossRef]